Bioactive Materials 6 (2021) 2983–2998

Contents lists available at ScienceDirect

Bioactive Materials

journal homepage: www.sciencedirect.com/journal/bioactive-materials

Surface modification of electrospun fibers with mechano-growth factor for mitigating the foreign-body reaction

Yang Song [a,b,c], Linhao Li [a,*], Weikang Zhao [d], Yuna Qian [e], Lili Dong [b], Yunnan Fang [a], Li Yang [a,b,**], Yubo Fan [a,***]

[a] Key Laboratory for Biomechanics and Mechanobiology of Ministry of Education, Beijing Advanced Innovation Center for Biomedical Engineering, School of Biological Science and Medical Engineering, Beihang University, Beijing, 100083, PR China
[b] Key Laboratory of Biorheological Science and Technology, Ministry of Education, Bioengineering College, Chongqing University, Chongqing, 400030, PR China
[c] Department of Bioengineering, University of California, Los Angeles, CA, 90095, USA
[d] Department of Orthopedics, The First Affiliated Hospital of Chongqing Medical University, Chongqing, 400016, PR China
[e] Wenzhou Institute, University of Chinese Academy of Sciences, Wenzhou, 325001, PR China

ARTICLE INFO

Keywords:
Mechano-growth factor (MGF)
Silk
Macrophage polarization
Foreign-body reactions (FBR)
Electrospinning

ABSTRACT

The implantation of synthetic polymeric scaffolds induced foreign-body reaction (FBR) seriously influence the wound healing and impair functionality recovery. A novel short peptide, mechano-growth factor (MGF), was introduced in this study to modify an electrospun polycaprolactone (PCL) fibrous scaffold to direct the macrophage phenotype transition and mitigate the FBR. *In vitro* studies discovered the cell signal transduction mechanism of MGF regulates the macrophage polarization via the expression of related genes and proteins. We found that macrophages response the MGF stimuli via endocytosis, then MGF promotes the histone acetylation and upregulates the STAT6 expression to direct an anti-inflammatory phenotype transition. Subsequently, an immunoregulatory electrospun PCL fibrous scaffold was modified by silk fibroin (SF) single-component layer-by-layer assembly, and the SF was decorated with MGF via click chemistry. Macrophages seeded on scaffold to identify the function of MGF modified scaffold in directing macrophage polarization *in vitro*. Parallelly, rat subcutaneous implantation model and rat tendon adhesion model were performed to detect the immunomodulatory ability of the MGF-modified scaffold *in vivo*. The results demonstrate that MGF-modified scaffold is beneficial to the transformation of macrophages to M2 phenotype *in vitro*. More importantly, MGF-functionalized scaffold can inhibit the FBR at the subcutaneous tissue and prevent tissue adhesion.

1. Introduction

Biomaterials based on synthesis and natural polymers have important clinical applications as basic carriers and functional support in biomedical fields such as regenerative medicine, drug delivery, and implants [1]. However, long-term implantation of biomaterials in the human body often causes aseptic inflammation, tissue adhesion, and fibrosis of surrounding tissues, resulting in post-surgical tissue adhesion, tissue functional decline, and implants failure, which increases the risk of secondary surgical removal for patients [2,3]. Therefore, the interaction of biomaterials with tissues and cells has always been the research focus of scientists. In the process of biomaterial design, in addition to considering the target functionality and structural stability, it is also necessary to fully understand the compatibility and tolerance between the host and the foreign material from a biological perspective [4].

The biomaterial/tissue foreign-body reaction process is mainly summarized into the following 4 steps: First, at the initial stage of material implantation, free proteins in the microenvironment of surrounding tissues (such as immunoglobulin, etc.) rely on non-specific adsorption to form inflammatory signals on the surface of the material; Second, after entering the acute inflammation, inflammatory cells such as neutrophils and macrophages in the body fluid recognize the

Peer review under responsibility of KeAi Communications Co., Ltd.
* Corresponding author. School of Biological Science and Medical Engineering, Beihang University, PR China.
** Corresponding author. Bioengineering College, Chongqing University, PR China.
*** Corresponding author. School of Biological Science and Medical Engineering, Beihang University, PR China.
E-mail addresses: linhaoli@buaa.edu.cn (L. Li), yanglibme@cqu.edu.cn (L. Yang), yubofan@buaa.edu.cn (Y. Fan).

https://doi.org/10.1016/j.bioactmat.2021.02.020
Received 17 December 2020; Received in revised form 31 January 2021; Accepted 16 February 2021

inflammatory signals and adhere to the surface of the material; third, the macrophages secrete inflammatory factors and chemokines to recruit and promote differentiation of myofibroblasts; finally, collagen fibrous capsule are formed on the surface of the material [3,5]. The collagen capsules can block the communication between the material and the peripheral tissues and cause the implants failure, tissue adhesion and hyperplasia. Importantly, macrophages play a key role in the process of foreign-body reaction. They can accelerate the degradation of materials through endocytosis and oxidative stress, regulate the transition between acute and chronic inflammation through polarization, and stimulate the recruitment and differentiation of myofibroblasts by secreting related cytokines [6,7].

Macrophages are the principal source of the first line of host defense that trigger inflammation, which also perform homoeostatic functions, including wound healing and tissue integrity maintaining [8]. Activated macrophages have been classified as different subtypes, during the innate immune response and inflammation by the invasion of foreign implants such as materials or virus, inflammatory cytokines such as tumor necrosis factor (TNF) and interferon gamma (IFN-γ) activate macrophages as pro-inflammatory M1 phenotype, which are implicated in phagocytosis and initiating inflammation. By contrast, activation by interleukin-4 (IL-4) or IL-13 polarizes macrophages as anti-inflammatory M2 macrophages, which have anti-inflammatory property and are involved in tissue homoeostasis [9]. In further research, it was found that by adjusting the polarization of macrophages, the FBR caused by materials implantation can be improved. The proportion, duration, and distribution of M1/M2 phenotypes of macrophages can significantly affect the degree of the FBR. The stimulation of persistent inflammatory signal can make macrophages stay in the M1 phenotype for a long time, which in turn will strengthen the later FBR [10–12]. Thus, to mitigate the FBR, effectively regulate the macrophages phenotype transition from M1 to M2 is an important strategy. Also, it can promote the tissue regeneration, as well as terminate the over-/chronic-inflammation during wound healing. Physical factors of biomaterials such as surface topography, pore size, and particle size can adjust the microphage polarization, and the use of immune regulatory factors such as IL-4 has also achieved good effects [10,13–16].

The electrospun nanofibrous three-dimensional matrix can simulate the structure and mechanical properties of the extracellular matrix and have obtained wide attention in the fields of tissue regeneration and drug delivery [17–19]. However, nanofibers have an ultra-high specific surface area, which can cause strong non-specific protein adsorption and can easily trigger a FBR at the interface between the material and tissue after being implanted *in vivo* [20–22]. Studies have shown that the surface topology factors of nanofibrous scaffold (such as aligned or randomly oriented nanofiber, pore size and fiber diameter) can affect the macrophages M1/M2 phenotypes transition, and increasing surface hydrophilicity can significantly reduce protein adsorption, the adhesion of inflammatory cells, and mitigate unwanted immune response [22–26]. In our previous work, we found that high-molecular-weight hyaluronic acid and natural silk protein can reduce the surface protein adsorption of electrospun scaffolds, and have an immunosuppressive effect on the FBR caused by implantation in rats [27]. However, due to the rapid degradation of hyaluronic acid, it is still difficult to achieve long-term effects for the material-tissue interface immunomodulation through the hydrophilic natural polymer composite system. We further modified the immunoregulatory factor IL-4 on the surface of electrospun nanofibers through click chemistry and silk layer-by-layer self-assembly technology, which can regulate the transition of macrophages from M1 to M2 phenotype in the early stage of implantation, thereby effectively reducing formation of collagen fibrous capsule and foreign-body giant cells at the late stage [28]. However, the surface modification of scaffolds by immunoregulatory factors has certain limitations. For example, IL-4 has a short half-life *in vivo* and excessive release can cause more serious tissue fibrosis.

Mechano growth factor (MGF) is one of the alternative splicing products of total insulin-like growth factor 1 (IGF-1), which forms when IGF-1 splice variants of Exon 4 spliced to Exon 5 (or Exon 6), and contains 24 peptides in human and 25 peptides in rodent [29,30]. Early studies have demonstrated that MGF is responsible for cell proliferation, migration, and stem cell differentiation, which has been wildly studied in tissue repair and disease prevention, such as tendon injury repair and bone regeneration [31–34]. To investigate the role of MGF in preventing knee osteoarthritis, we found that MGF can inhibit inflammatory cytokine production in human synoviocytes of knee osteoarthritis, such as IL-1β and TNF-α [35]. Additionally, a study on rabbit knee joint osteoarthritis, we found that MGF joint cavity injection will not only prevent cartilage degradation, but also relief the inflammation induced arthrocele [36]. These findings indicate that MGF not only promotes tissue repair, but also has the potential to regulate the inflammatory microenvironment *in vitro* and *in vivo*. Therefore, we propose a hypothesis that MGF may have immunomodulatory ability that can regulate the macrophage polarization to mitigate the FBR.

The silk fibroin layer-by-layer assembly capsules and surface modification have been shown to safeguard the activity of sensitive biological agents against harsh environmental conditions in our previous study [37]. Furthermore, click chemistry was introduced to fabricate biomolecule/polymer bioconjugation with controllable properties [38,39]. By introducing the click chemistry technique in preparing functional biomaterials, the accuracy and controllability of the bioconjugation reaction can be effectively improved [40]. Hence, applying "click" chemical conjugation to the SF surface modified electrospun fibers may provide multiple approaches for localizing cell signals and factors immobilization. In the present study, the mechanism of how MGF modulate macrophage polarization was uncovered on epigenetic-scale. Next, in order to verify the influence of MGF on the FBR caused by implantation, we developed a silk surface-functionalized electrospun polycaprolactone (PCL) fibrous scaffolds and decorated with MGF by CuAAC click chemistry. The effects of MGF decorated nanofibrous scaffolds on the macrophage polarization *in vitro* and *in vivo*, foreign-body reaction, and related molecular mechanisms were investigated and discussed. Finally, we used electrospun scaffolds as a physical barrier against tissue adhesion in a rat tendon repair model to verify the anti-adhesion effect of MGF surface modification.

2. Material and methods

2.1. Cell culture and treatment

RAW264.7 mouse macrophages (ATCC, USA) were cultured in Dulbecco's Modified Eagle's Medium (DMEM) (Gibco Life Technology, USA) supplemented with 20% fetal bovine serum (FBS, Gibco, USA). The electrospun nanofibrous scaffolds were immersed in 70% ethanol for 30 min and dried under sterile conditions and exposed to UV radiation for 1 h; then, the scaffolds were washed 3 times with PBS for 20 min each and incubated with serum-free DMEM for 24 h before cell seeding. The cells were seeded onto the nanofibrous scaffolds in a 24-well plate at a density of 1×10^5 cells/well and cultured with DMEM and 20% FBS at 37 °C, 5% CO_2 and 95% humidity. To determine the effect of MGF on macrophage polarization, 10 ng/mL, and 20 ng/mL MGF-C25E (Phoenix Pharmaceuticals Inc., USA) was used for cell treatment and nanofiber modification. Additionally, to determine the role of histone acetylation in MGF regulate macrophage polarization, histone de acetyltransferase inhibitor valproic acid (VA, 0.5 mM, Sigma, USA) and histone acetyltransferase inhibitor anacardic acid (AA, 1 μM, Sigma, USA) were used for cell treatment.

2.2. Quantitative real-time polymerase chain reaction (qRT-PCR)

Total RNA was isolated from the collected cells using a MagMAX™-96 Viral RNA Isolation Kit (Thermo Fisher, USA) and then reverse transcribed into complementary DNA (cDNA) with a high-capacity

cDNA reverse transcription kit (Life Technologies, USA) according to the manufacturer's protocol. qRT-PCR was performed with the TaqMan™ PreAmp Master Mix (Life Technologies). qRT-PCR was performed in a 20 μL volume with 0.5 μL of each primer and a 1 μL cDNA sample. The reaction was initiated by activating the polymerase with a 5 min pre-incubation at 95 °C. Amplification was achieved with 40 cycles of 15 s denaturation at 95 °C, 1 min annealing at 60 °C, and 10 s extension at 72 °C. Relative gene expression data was analyzed using the $2^{-\Delta\Delta CT}$ method. Each sample was analyzed in triplicate. All the primers were purchased from ThermoFisher (USA). The primer sequences are shown in Table S1 (Supplementary information).

2.3. Cell morphology

To determine the cell-scaffold interaction, the morphology of cells on cell-culture dish and scaffolds was detected by confocal laser scanning microscopy (CLSM, Leica, Germany). Macrophages cultured on scaffolds at a density of 1×10^4 cells per well for 48 h and fixed with 3.7% formaldehyde in PBS for 15 min, rinsed in PBS and permeabilized with 0.2% Triton X-100 for 5 min. Samples were then rinsed with PBS and incubated with 1 mg/mL Alexa Fluor 488-phalloidin (Life Technologies) and 10 μg/mL Alexa Fluor 594-wheat germ agglutininat (WGA) respectively for 30 min at room temperature to stain cytoskeleton and cytomembrane. After washing with PBS, the cells were mounted with mounting media containing DAPI (Sigma-Aldrich, USA) for nuclei staining. Fluorescent images from stained scaffolds were obtained using CLSM. Cell roundness was measured by the Image J software (USA) to assess cellular deformation: Roundness = $\text{Perimeter}^2/(4\pi \times \text{Area})$.

2.4. Immunofluorescent staining

To detect polarization of macrophages, macrophages were seeded on glass slides or scaffolds. After treated by MGF, different samples were removed from cell culture medium and fixed with 3.7% formaldehyde in PBS for 15 min, rinsed in PBS and incubated with 2% BSA +0.2% Triton X-100 in PBS for 60 min. Then rinsed in PBS and incubated with primary antibody (CD68, CD86, CD163, CCR7, CD206, iNOS, Arg-1, 1:50–1:100) at 4 °C overnight, followed by a 1 h treatment with Alexa Fluor 488/555-labled secondary antibody. Finally, samples were rinsed with PBS and stained with 0.5 mg/mL DAPI (Sigma-Aldrich, USA) at room temperature for 15 min. Fluorescent images from stained scaffolds were obtained using CLSM. Both primary antibodies and secondary antibodies for immunofluorescence were purchased from Abcam (USA). To detect the histone acetylation and DNA methylation, after MGF treatment, samples were collected and cover cells completely with ice-cold 70% ethanol for 5 min and incubate samples in 1.5 M HCl for 30 min at room temperature to active the 5 mC. Then block samples in 5% NDS for 60 min and incubate with ACH3 primary antibody (1:400, Abcam, USA) and 5 mC (1:1000, Cell signaling technology, USA) at 4 °C overnight, followed by a 1 h treatment with Alexa Fluor 488/555-labled secondary antibody. Finally, samples were rinsed with PBS and stained with 0.5 mg/mL DAPI (Sigma-Aldrich, USA) at room temperature for 15 min. Fluorescent images from stained scaffolds were obtained using CLSM.

2.5. Enzyme-linked immunosorbent assay (ELISA)

The 5 mC level (EpiGentek, USA), HAT activity (EpiGentek, USA), TGF-β1 and TNF-α (R&D systems, USA) concentration were detected by ELISA kits. Simply, after cells treated by MGF for 2 days, DNA and nuclear extracts were collected by DNA extraction kit (ThermoFisher Scientific, USA) and nuclear extraction kit (EpiGentek, UAS), then 100 ng DNA was used to detect the 5 mC level and 5 μg nuclear extraction was used to detect the HAT activity follow with instruction. For TGF-β1 and TNF-α quantification, 1×10^5 cells cultured in 6 cm tissue-culture dish and treated with or without MGF for 5 days, then the culture medium were collected and 100 μL medium were used for concentration test. The results were measured by microplate reader (Bio-Rad, USA) at 450 nm wavelength.

2.6. Single cell force spectroscope

To determine whether macrophages have MGF receptor on cell membrane, the single cell adhesion force between cell and scaffolds were detected by single cell force spectroscopy as previous reported [39]. Simply, Bruker tipless AFM cantilever NPO-10 (k = 0.06 N/m) coated with ConA for 30 min, and then wash by PBS for 3 times. The AFM cantilever attach a single cell by performing an approach-retract cycle on glass slide and then adjust the contact force = 2 nN, record F–D curves for contact times = 0 s, 10 s and 30 s on MGF, IGF-1 and non-coated glass slides. Bruker data processing software was used to process an F–D curve and obtained the value of initial attachment.

2.7. Western blotting

The protein concentration of each sample was measured using a bicinchoninic acid (BCA) protein assay kit (Bioteke, China). Equal amounts of total protein (50 μg) from each sample were separated in a 10% SDS-PAGE gel and transferred to a PVDF membrane at 120 V for 2 h at room temperature (RT). The blot was blocked with 5% nonfat dry milk suspended in 1x TBS (25 mM Tris, 137 mM NaCl, and 2.7 mM KCl) for 1 h at room temperature. Membranes were incubated with primary antibodies against STAT6 and GAPDH (Cell Signaling Technology, USA). The resulting blots were incubated with 1:1,000 rabbit–mouse secondary antibodies (Cell Signaling Technology, 4414/4410, USA). Bands were scanned using a densitometer (Bio-Rad) and quantified using the Quantity One 4.6.3 software (Bio-Rad).

2.8. STAT6 knockdown

Macrophages were seeded in 6 cm dish with 1×10^5 cells per well. After 24 h of seeding, an siRNA transfection reagent was added to the cell culture medium. The siRNA transfection reagent was prepared as per specification. Simply, 2.5 μL of the X-tremeGENE siRNA transfection reagent (Roche, 4476115001, Switzerland) was pipetted into 47.5 μL Opti-MEM I medium (ThermoFisher, 31985062, USA), then 0.5 μg of STAT6 siRNA (Cell Signaling Technology, 9024, USA) was directly pipetted into the above medium, and the tube was mixed and incubated for 20 min at 25 °C. Then the siRNA transfection reagent was added into a 2 mL growth medium (one well), and the cells were returned to the incubator overnight. After transfection, the medium was replaced with a serum-containing cell culture medium and the protein knockdown was measured after 72 h.

2.9. Preparation of electrospun scaffolds

PCL nanofibers were prepared by electrospinning. PCL solution was prepared by dissolving 1 g of PCL (90 kDa, Sigma, USA) in 10 mL of hexafluoroisopropanol (HFIP, Sigma, USA) to form a 10% (w/v) solution. Electrospinning was performed in a fume hood using an open-cage target to collect fibers. To purify the SF, cocoons from B. mori (Chongqing Sericulture Science and Technology Research Institute, China) were boiled twice in an aqueous solution of 0.02 M Na_2CO_3 (Sigma, USA) for 1 h, rinsed 3 times with ultrapure water and dissolved in 9.3 M LiBr (Sigma, USA) at 55 °C to generate a 10% (w/v) solution. This solution was dialyzed (MWCO = 3500 Da, Pierce Chemical, USA) against ultrapure water for 3 days by changing the water daily to remove the ions and other impurities. The solution was collected, filtered, and stored at 4 °C.

The coupling of azido functional groups to the SF (Azido-SF) was performed using a diazonium coupling reaction. In brief, 0.360 mM 4-azidoaniline hydrochloride (Sigma) was dissolved in 1 mL of a 1:1 acetonitrile/water solution, which was then mixed with 0.5 mL of a p-

toluenesulfonic acid monohydrate (1.430 mM, Sigma) solution dissolved in water. Finally, sodium nitrite (0.715 mM, Sigma) dissolved in 0.5 mL of water was added to the mixture. All the solutions were prepared in an ice bath before mixing. The diazonium coupling reaction was started by adding 2 mL of a 50 mg/mL borate-buffered SF solution (pH = 9), and the reaction could proceed for 30 min at room temperature; the solution was then dialyzed against ultrapure water. The alkyne-MGF (A-MGF) conjugates were synthesized via EDC/NHS coupling. EDC (2 mM) and NHS (5 mM) were added to the 1 mg/mL of MGF-Cysteine (1 mM, Sangon, China) in MES buffer (0.1 M, pH = 6), followed by the addition of 1.5 mM I-PEG4-alkyne (Sigma) and reaction for 12 h at 25 °C under stirring. The resulting solution was dialyzed (MWCO = 1 kDa) against ultrapure water.

SF LbL coating was used to modify the PCL nanofibers at an SF concentration of 1 mg/mL. PCL nanofibrous scaffolds were cut into 3 × 3 cm^2 rectangular shapes and washed 3 times by ultrapure water. Prior to SF deposition, 1 mL of a 0.5 mg/mL aqueous solution of bPEI25 was added to the PCL nanofibers and incubated for 15 min at room temperature. After being washed three times, the nanofibers were incubated with 1 mg/mL SF solution for 15 min at 4 °C. Assembly at low temperature was used to ensure SF protein stability and to decrease protein precipitation. The SF-coated PCL nanofibers were immersed in 90% methanol for 15 min to induce silk crystalline b-sheet structure formation. The washed nanofibers were then dried under nitrogen gas flow at 15 kPa and subjected to the next coating procedure until the desired number of layers was deposited. The A-SF/A-MGF conjugates were synthesized by CuAAC between the A–SF–coated nanofibers and the A-MGF solution. In brief, the synthesis was performed in a total volume of 2 mL for each reaction, in which the A-MGF solution (1 mg/mL, pH = 7.0) was mixed with sodium ascorbate (0.2 mM, Sigma), $CuSO_4$ (0.1 mM, Sigma) and TBTA (0.02 mM, Sigma). The mixture was added to the A-SF coated PCL nanofibers, reacted under nitrogen gas for 24 h, and washed thoroughly by ultrapure water.

2.10. Characterization of nanofibrous scaffolds

The morphology of nanofibrous scaffolds was characterized by field emission SEM (Zeiss Auriga crossbeam system, Germany) with an accelerating voltage of 5 kV after the samples were coated with gold. Fluorescence images of FITC–SF–coated nanofibers were obtained using a Leica DMI6000 (Wetzlar, Germany) confocal microscope. Quantitative fluorescence intensity was obtained from the images by straight line profiling of a commercial software (Image Pro Plus, IPP 6.0, Media Cybernetics, USA).

Chemical analysis results of the SF, azido-SF, alkyne-MGF-click-azido-MGF solutions were recorded on a GENESYS 10S UVeVis spectrometer (Thermo Scientific, Waltham, MA) over a range of 190–600 nm. The efficiency of the diazonium coupling reaction was assessed by UV absorbance at 352 nm (A-SF).

Chemical and structural analyses of the SF and A-SF powder were performed by FTIR spectroscopy over a range of 4000–400 cm^{-1}. The FTIR spectra of different samples were obtained by a Nicolet spectrometer system (System 2000, PerkinElmer) with a DTGS KBr detector.

2.11. Subcutaneous implantation

The ethics committee of Third Military Medical University (Chongqing, China) approving the experiments and all *in vivo* experiment were performed in accordance with relevant guidelines and regulations. The scaffolds were folded into a square shape with dimensions of 10 mm × 10 mm × 100 μm (L × W × T) under sterile conditions. Twenty male 3-month-old Sprague-Dawley rats (body weight, around 220 g) were individually housed in wire-bottom cages in temperature- and light-controlled rooms. The use of rats conformed to the Guiding Principles for the Care and Use of Animals of our Institute and was approved by the Animal Care and Use Committee of our Institute. The animals were anaesthetized with 0.3% pentobarbital sodium (0.5 mL/100 g, Shanghai Pharma, China). Four small midline incisions were made on the dorsum of each rat, and the scaffolds were introduced in lateral subcutaneous pockets created by blunt dissection. Procaine penicillin (20 mg/kg) was given intramuscularly preoperatively and after the operation for prophylactic infection control. Both animals remained in good general health throughout the study, as assessed by their weight gain. After 14 and 28 days, the rats were sacrificed, and the implanted scaffolds were removed en-bloc with the naturally surrounding tissue. The samples were fixed and processed for histology, as described below. At every time point, four replicates of each type of nanofibers were implanted into four different rats to provide statistical significance in the histological studies.

2.12. Tendon adhesion

The ethics committee of Third Military Medical University (Chongqing, China) approving the experiments and all *in vivo* experiment were performed in accordance with relevant guidelines and regulations. 24 male SD rats, weighing around 250 g, were used for tendon anti-adhesion assay. Rats were anaesthetized by intramuscular injection of ketamine (20 mg/kg). A midline incision was made in the skin over the Achilles tendon. The tendon was vertical cutting following the orientation of endotenon approximately 5 mm from the calcaneal bone to mimic the tendon rupture. Then the injured tendon was wrapped by fibrous scaffold. The animals were random Ly assigned to three groups; each group has 8 rats. No treatment was performed as control group I.

2.13. Statistical analysis

The results are expressed as the mean ± standard deviation (SD). Statistical analysis was performed using Student's t-test as well as one-way analysis of variance (ANOVA) followed by the Tukey HSD test for post hoc comparisons (OriginLab, OriginV8.0 Software). Differences were considered significant when $p < 0.05$.

3. Results

3.1. MGF promotes macrophage polarization toward an anti-inflammatory phenotype

To determine the effect of MGF on the polarization of macrophages, mouse macrophages cell line, RAW 264.7, were synchronized in the G0/G1 phase of the cell cycle and seeded at a density of 1 × 10^5 cells/cm^2 onto glass coverslips. Then 10–20 ng/mL MGF were used for cell treatment. After 72 h, cells were fixed and immunocytochemically stained for macrophage phenotype markers including CD68 as a pan-macrophage lineage marker, CD86 and CCR7 as pro-inflammatory markers (M1), CD163 and CD206 as anti-inflammatory markers (M2) to quantitatively analyze the tendency of macrophage polarization. As Fig. 1a and b shown that both 10 and 20 ng/mL MGF treatment can significantly increase the number of anti-inflammatory macrophages, but does not affect the expression of M1 related markers. Gene levels of macrophage anti-inflammatory markers, CD163 and CD206, also increased significantly after MGF treated for 2, 6, and 12 h (Fig. 1c and Supplementary Fig. 1). In addition, the cell morphology changes after MGF treatment for 24 h (Fig. 1d). As Fig. 1 e and **f** shown, 10–20 ng/mL MGF treatment can significantly decrease the cell circularity and the cell area, the elongated cell shape indicates that macrophages have undergone cytoskeletal rearrangement, resulting in the morphological characteristics of anti-inflammatory phenotype. To investigate the MGF how to regulate macrophages polarized into M2 phenotype, RNA sequencing was performed to analysis macrophages treated by MGF for 12 h. Hierarchal clustering analysis shown that after MGF treatment, *kcnq1* and *folr2*, genes correlated with endocytosis reveals significant differences (Fig. 1g). This result indicates that macrophages' response to the stimuli

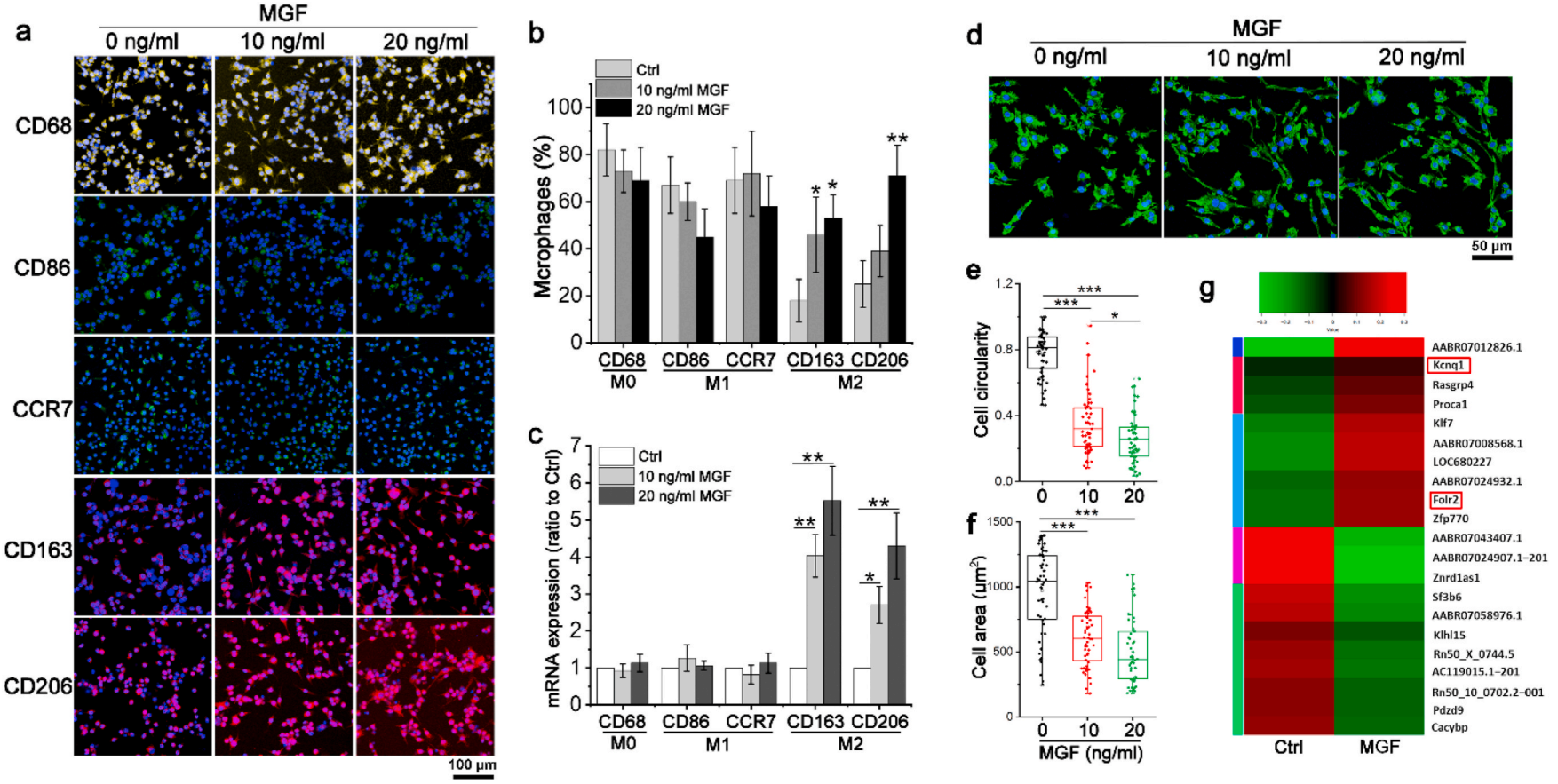

Fig. 1. MGF promotes macrophage polarization toward anti-inflammatory phenotype.

from MGF could depend on cell endocytosis.

(a) Immunofluorescent images of macrophages stained with pan-macrophage marker CD68, pro-inflammation phenotype markers CD86 and CCR7, and anti-inflammation phenotype markers CD163 and CD206 after 0, 10, and 20 ng/mL MGF treatment for 72 h. **(b)** Image analysis the percentages of $CD68^+$ pan-macrophage, $CD86^+$, and $CCR7^+$ pro-inflammatory macrophages, and $CD163^+$ and $CD206^+$ anti-inflammatory macrophages after different doses of MGF treatment for 72 h *p < 0.05, **p < 0.01. Data are presented as the mean ± SD (n = 3). **(c)** Gene expression of CD68, CD86, CCR7, CD163 and CD206 in macrophages differentiated after different doses of MGF treatment for 12 h. Results were normalized to an endogenous control gene (GAPDH) and expression relative to non-treatment group. *p < 0.05, **p < 0.01. Data are presented as the mean ± SD (n = 3). **(d)** Cell morphology was stained by Alexa Fluor 488-phalloidin after different doses of MGF treatment for 24 h. **(e)** Cell circularity and **(f)** cell area analysis of macrophages after MGF treatment for 24 h *p < 0.05, ***p < 0.001. Data are presented as the mean ± SD (n = 100). **(g)** Heat map indicating the change in the expression of significant difference genes after MGF treatment for 12 h (red: high expression; green: low expression). Red frames indicate the genes related to endocytosis.

3.2. Macrophages response to MGF stimuli by clathrin-mediated endocytosis

RNA sequencing shows that *kcnq1* expression on MGF-treated groups are significantly higher than non-treated group, which correlated with clathrin-mediated endocytosis (Fig. 1g). To determine whether macrophages' response to MGF stimuli depends on endocytosis, MGF-GFP peptide was used as a fluorescent indicator for observation. As Fig. 2a shown, MGF-GFP was phagocytosed by macrophages after treatment for 2 h. To further determine the endocytosis is mediated by clathrin, dynoser I as the specific inhibitor was used to treat macrophages for 24 h. As Fig. 2b and c shown, after clathrin inhibition, MGF cannot change the macrophages morphology, the cell circularity has seldom difference in dynoser I pre-treated groups with and without MGF treatment. We did not find any changes in cell morphology by adding inhibitors of other endocytosis mechanisms for 24 h treatment, such as micropinocytosis inhibitor wortmannin and caveolae-mediated endocytosis inhibitor filipin (Supplementary Fig. 2). Additionally, compared with the dynoser I untreated MGF groups, the protein expression of the M2 marker (CD206) in the clathrin-mediated endocytosis inhibited groups were significantly down-regulated (Fig. 2d, e, and 2f). Furthermore, qRT-PCR results shown that after cellular endocytosis inhibited by dynoser I, MGF treatment cannot induce anti-inflammation macrophages related markers expression (Fig. 2f). These results indicate that macrophages respond to MGF stimuli by clathrin-mediated endocytosis. We also detected the cell adhesion force on MGF-coated glass slide suggests that macrophages may not have specific MGF receptor on the cell membrane, which further support that macrophage endocytosis may play an important role in response the MGF stimuli (Supplementary Fig. 3).

(a) Immunofluorescent images of macrophage endocytosis of MGF, cell plasma membrane was stained by Alexa Fluor 594-WGA (red), and MGF-GFP (green) was detected in the cytoplasm. Scale bar, 20 μm. (b) Macrophages morphology was stained by Alexa Fluor 594-WGA and Alexa Fluor 488-phalloidin after pretreated by dynoser I (endocytosis inhibitor) for 24 h and then treated by different doses of MGF for 24 h. Scale bar, 50 μm. (c) Cell circularity analysis of macrophages after MGF treatment for 24 h **p < 0.01. Data are presented as the mean ± SD (n = 3). (d) Immunofluorescent images of macrophages stained with M1 phenotype marker iNOS, and M2 phenotype marker CD206 after non-treatment, MGF treatment, and pretreated by dynoser I then treated by MGF for 72 h. Scale bar, 100 μm. (e) Image analysis the percentages of $CD206^+$ macrophages and $iNOS^+$ macrophages after dynoser I and MGF treatment. *p < 0.05. Data are presented as the mean ± SD (n = 3). (f) Gene expression levels of CD86, CCR7, CD163, and CD206 in macrophages differentiated after pretreated by dynoser I for 24 h and 12 h culturing with MGF. Results were normalized to an endogenous control

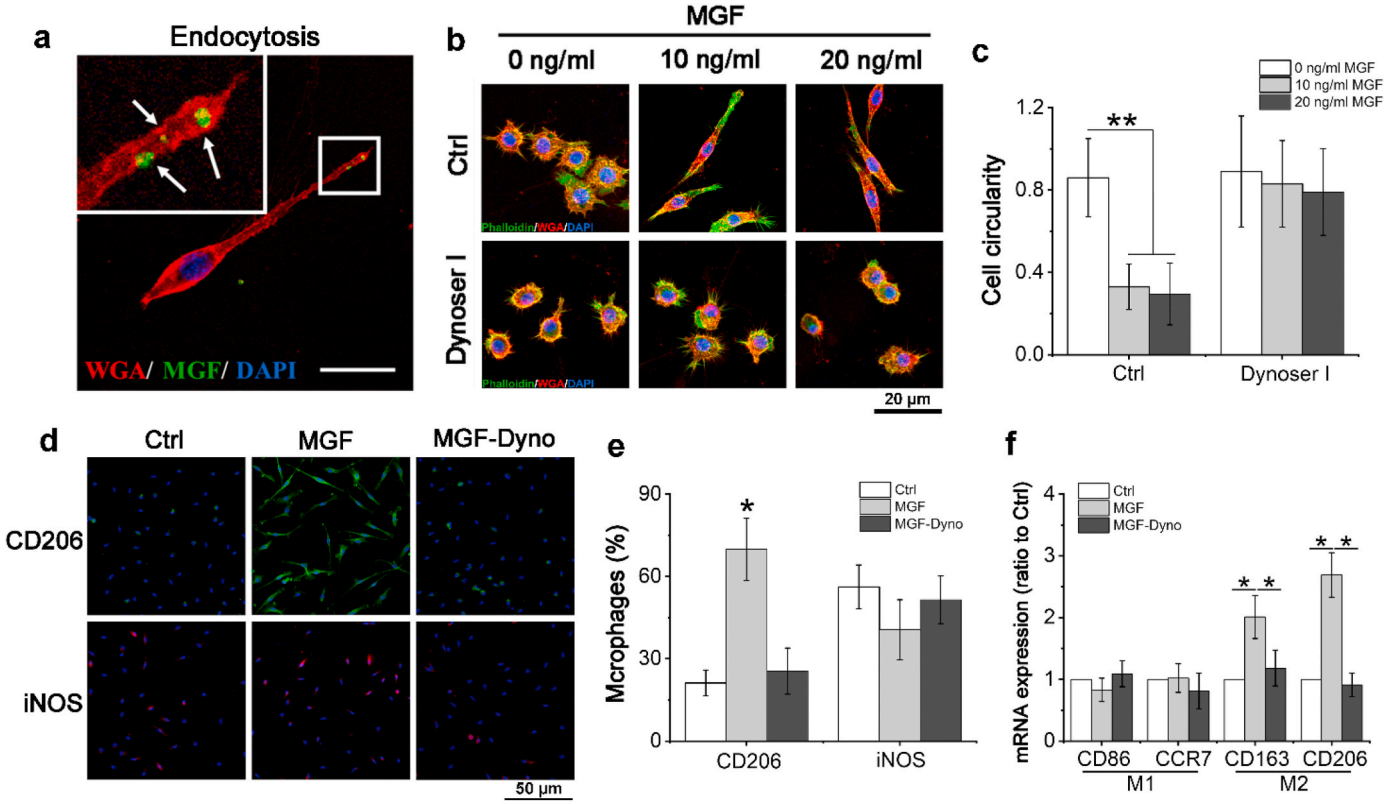

Fig. 2. Macrophages response to MGF stimuli by clathrin-mediated endocytosis.

gene (GAPDH) and expression relative to non-treatment group. *p < 0.05. Data are presented as the mean ± SD (n = 3).

3.3. MGF promotes histone acetylation to regulate macrophage phenotype transition

To determine the MGF how to regulate the pan-macrophage polarized into anti-inflammation phenotype, the histone acetylation change have been detected after cell treated by MGF. As Fig. 3a shown that after 24 h treatment, the level of AcH3 in MGF-treated macrophages is significantly higher than non-treated group, WB result further prove that MGF can increase the AcH3 in MGF-treated macrophages (Fig. 3b and c). However, DNA methylation was not detected in MGF-treated macrophages (Supplementary Fig. 4). These results suggest that MGF could transform chromatin structure from tightly closed to loosely open in pan-macrophages via histone acetylation, result in promoting macrophage phenotype transition. Additionally, to study MGF how to regulate the histone acetylation in macrophages, the activity of histone acetyltransferases (HATs) and histone deacetylases (HDACs) were detected in macrophages after treated by 20 ng/mL MGF for 24 h. As Fig. 3d and e shown that the HAT activity of MGF-treated cells was remarkably higher than non-treated cells. On the other hand, the HDAC activity been reduced by MGF treatment in macrophages. Furthermore, to investigate whether MGF is capable to promote macrophages polarization into anti-inflammation phenotype by regulating histone acetylation, HAT inhibitor anacardic acid (AA) and HDAC inhibitor valproic acid (VA) were used to pre-treatment macrophages for 24 h. The qRT-PCR results prove that HAT inhibition will eliminate the capability of MGF to induce anti-inflammation related genes expression in macrophages such as CD163 and CD206 (Fig. 3f). However, HDAC inhibition can promote the anti-

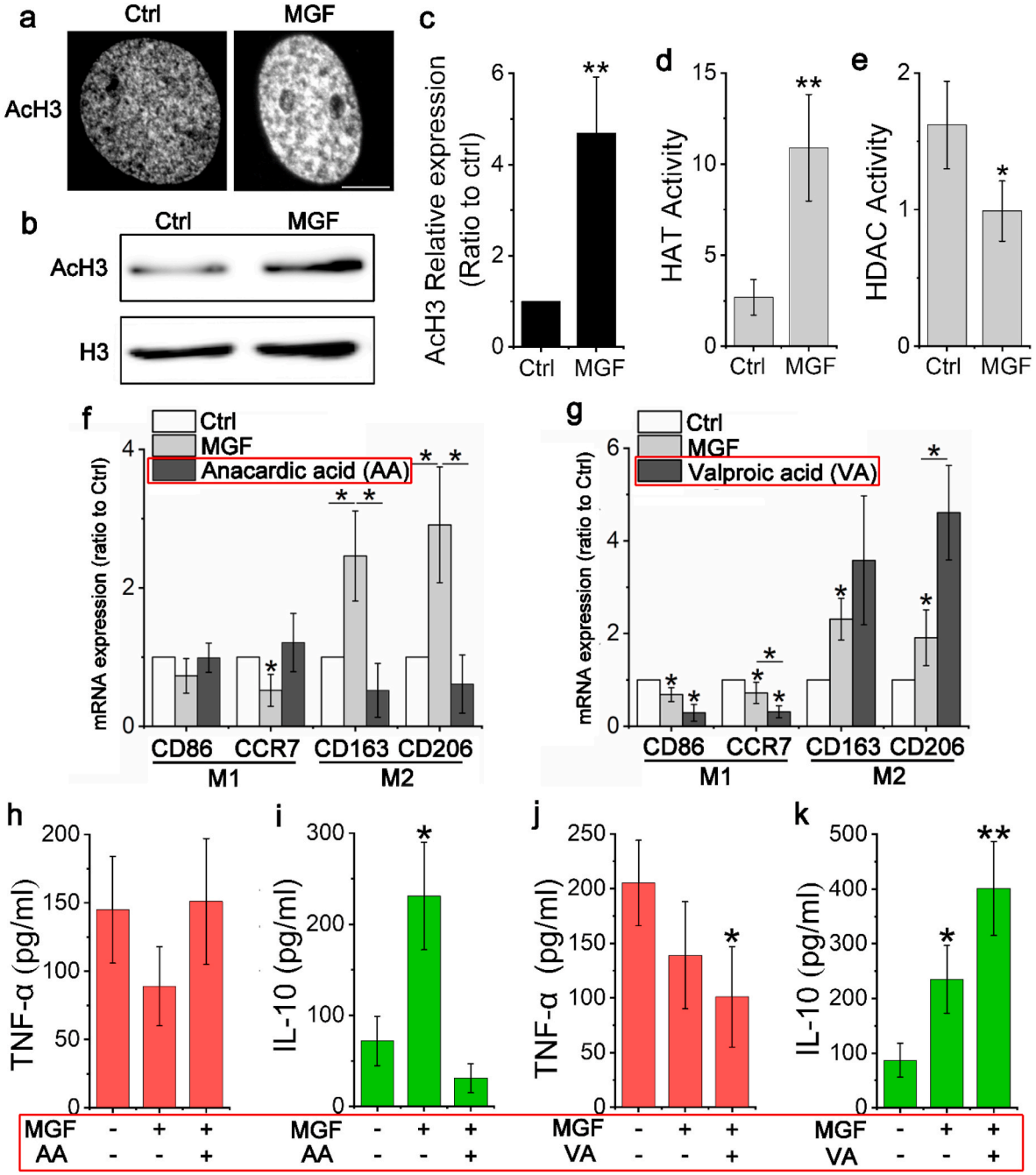

Fig. 3. MGF promotes histone acetylation to regulate macrophage phenotype transition.

inflammation related genes expression in macrophages, which is even higher than MGF treatment group (Fig. 3g). Inhibitors combine with MGF treat cells for 7 days, the macrophage phenotype changes were analysis by detect the secretion of TNF-α (pro-inflammation) and IL-10 (anti-inflammation). As Fig. 3h and i shows that MGF treatment can significantly increase the level of IL-10 but cannot reduce TNF-α secretion in macrophages. When the activity of histone acetyltransferases was inhibited, MGF can neither promote the expression of IL-10 nor reduce the level of TNF-α. On the contrary, when the activity of histone deacetylases was inhibited, MGF can significantly increase the secretion of IL-10, at the same time, MGF also can remarkably reduce the expression of TNF-α in macrophages (Fig. 3j and k). These results suggested that MGF can promote pan-macrophage polarization into anti-inflammation phenotype by regulating the histone acetylation.

(a) Immunofluorescent images of macrophage stained with AcH3 after non-treatment and MGF treatment for 24 h. Scale bar, 5 μm. (b) Western blot detected the levels of AcH3 in macrophages after treated by MGF for 24 h. (c) Identify the density value of Western blot to analysis the change of AcH3 in MGF-treated macrophages, non-treated cells act as control, and normalized the control as 1. **$p < 0.01$. Data are presented as the mean ± SD (n = 3). (d) and (e) ELISA detected the HAT and HDAC activity (OD/h/mg), **$p < 0.01$. Data are presented as the mean ± SD (n = 4). (f) Gene expression of CD86, CCR7, CD163 and CD206 in macrophages differentiated after pretreated by anacardic acid for 24 h and 12 h culturing with MGF. Results were normalized to an endogenous control gene (GAPDH) and expression relative to non-treatment group. *$p < 0.05$. Data are presented as the mean ± SD (n = 3). (g) Gene expression of CD86, CCR7, CD163 and CD206 in macrophages differentiated after pretreated by valproic acid (VA) for 24 h and 12 h culturing with MGF. Results were normalized to an endogenous control gene (GAPDH) and expression relative to non-treatment group. *$p < 0.05$. Data are presented as the mean ± SD (n = 3). (h) ELISA detected the TNF-α secretion after treated by anacardic acid and MGF. Data are presented as the mean ± SD (n = 3). (i) ELISA detected the IL-10 secretion after treated by anacardic acid and MGF. *$p < 0.05$. Data are presented as the mean ± SD (n = 3). (j) ELISA detected the TNF-α secretion after treated by valproic acid and MGF. *$p < 0.05$. Data are presented as the mean ± SD (n = 3). (k) ELISA detected the IL-10 secretion after treated by valproic acid and MGF. *$p < 0.05$, **$p < 0.01$. Data are presented as the mean ± SD (n = 3).

3.4. MGF promotes macrophage phenotype transition via STAT6

It is already understanding that STAT6 is a core factor to drive macrophage anti-inflammatory polarization. To study whether MGF regulates macrophage phenotype transition via STAT6, Western blot and immunostaining were used to analysis the STAT6 expression after MGF treatment. As Fig. 4a–c shows that MGF is capable to induce STAT6 expression and promote STAT6 relocation from cytoplasm to nucleus. In addition, STAT6 knockdown will block the effect of MGF in regulating macrophage polarization, such as promote the IL-10 secretion (Supplementary Fig. 5). Also, MGF cannot induce STAT6 expression in HAT-inhibited macrophages, and HDAC inhibition can further promote STAT6 expression in macrophages (Supplementary Fig. 6 and Fig. 7). These results suggest that pan-macrophages response the MGF stimuli via endocytosis, then MGF promote STAT6 activation and actin reorganization, these processes induce anti-inflammation phenotype related genes expression, such as CD206 and CD163. At the same time, MGF induces a more 'open' chromatin state by histone acetylation, which increases the accessibility of transcription complexes to genomic DNA. Therefore, MGF can promote the pan-macrophages polarization into anti-inflammation phenotype (Fig. 4d).

(a) Western blot detected the levels of STAT6 in macrophages after treated by MGF for 48 h. (b) Identify the density value of Western blot to analysis the change of STAT6 in MGF-treated macrophages, non-treated cells act as control, and normalized the control as 1. *$p < 0.05$. Data are presented as the mean ± SD (n = 3). (c) Immunofluorescent images of macrophage stained with STAT6 after MGF treatment for 48 h. Scale bar, 100 μm. (d) Potential signal pathways of macrophages affected by MGF. MGF was endocytosed by macrophage, which induces actin reorganization (morphological changes) and STAT6 activation. Meanwhile, MGF increased the level of histone acetylation and prepared an "open" chromatin state to promote anti-inflammatory phenotype genes expression.

3.5. MGF surface functionalization of electrospun PCL nanofibers via LbL SF deposition and click chemistry

The overall MGF modification process consisted of the following 3 steps: First, the thiol in the cysteine residue of MGF was reacted with iodide-PEG4-alkyne using a nucleophilic substitution reaction (Fig. 5a, Step 1). Second, the tyrosine residues of SF were chemically modified using diazonium coupling chemistry to add an azido moiety, as shown in Fig. 5a, Step 2. This reaction produced a dark brown SF solution and the rise of a new absorption band at 352 nm in the UV spectra and an additional characteristic peak at 2125 cm^{-1} in the FTIR spectra, indicating the reaction successfully attached the azido groups to the SF (Fig. 5b and c). Third, we used the azido-SF solution to coat the surface

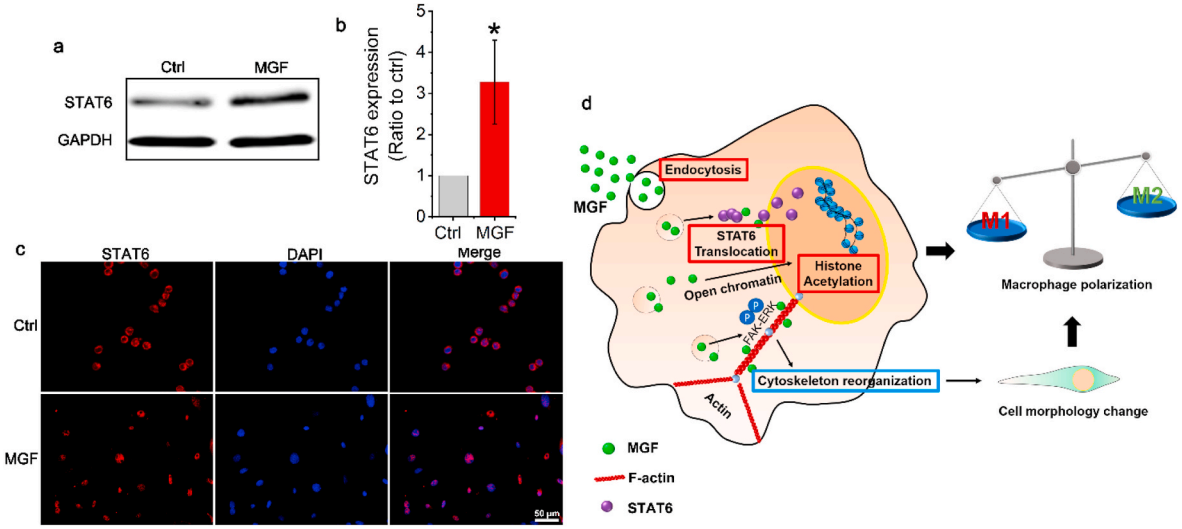

Fig. 4. MGF promotes macrophage phenotype transition via STAT6.

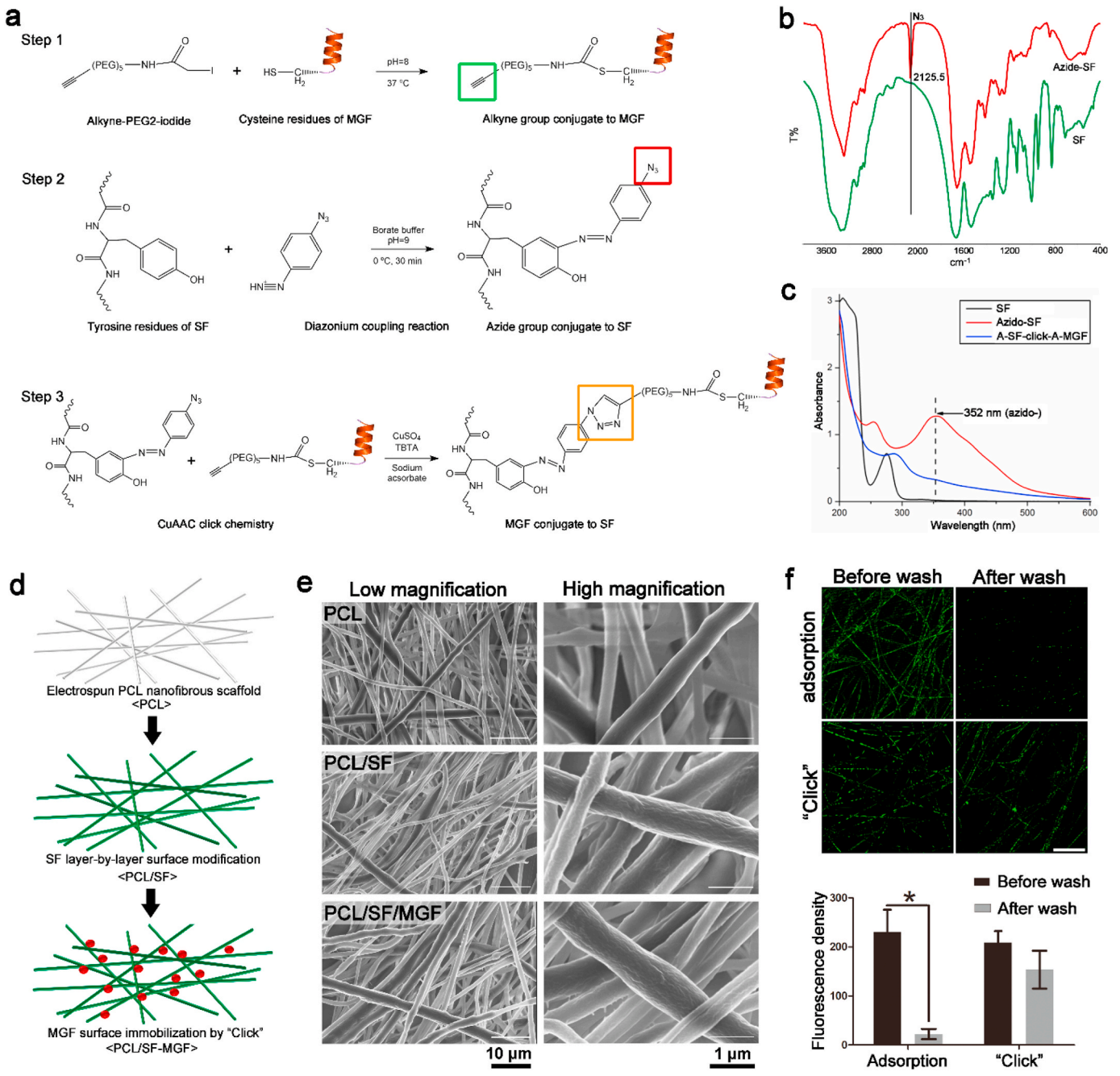

Fig. 5. MGF surface functionalization of electrospun PCL nanofibers via LbL SF deposition and click chemistry.

of electrospun PCL nanofibers via LbL assembly (Fig. 5d). For the click chemistry, the alkyne-MGF solution was reacted with the azido–SF–modified PCL nanofibers under Cu(I) catalysis overnight to generate PCL nanofibrous scaffolds with a surface covalently modified by MGF (Fig. 5a, Step 3 and 5d). After modification with MGF, the absorption band at 352 nm disappeared, indicating the CuAAC reaction successfully connected alkyne-MGF and azido-SF (Fig. 5c). SEM images showed a significant increase in the surface roughness of the PCL fibers after multiple SF layers deposition, but no difference was observed in the MGF modified scaffolds (Fig. 5e). We also measured the fluorescence density of FITC labeled MGF by CLSM to compare the stability of physical adsorption and click covalent linkage (Fig. 5f). After repeated PBS cleaning, it was almost difficult to find FITC-labeled MGF on the surface of the electrospun fibers in the adsorption group, but there was still a lot of green fluorescence in the click group. ImageJ software analysis of fluorescence intensity showed a markedly decreasing trend after PBS washing in the adsorption group. There was no significant difference in the fluorescence density of the click group before and after washing (Fig. 5f Bottom). The results showed that the MGF peptide can efficiently covalently attached to the SF-modified nanofiber surface.

(a) Chemical reactions of covalent bonding establishment between MGF and SF-modified PCL nanofibers by CuAAC click chemistry. Step 1: The addition of alkyne group to MGF using a nucleophilic substitution reaction. Step 2: The addition of azide group to SF tyrosine residues using a diazonium coupling reaction. Step 3: Covalent bonding of alkyne-MGF to LbL azide–SF–modified PCL nanofibers using CuAAC click chemistry. (b) FTIR spectrum analysis of SF and azide-SF powder. (c) The UV–Vis absorbance spectrum of pure SF, azide-SF, and azide–SF–click-alkyne-MGF samples from 200 to 600 nm. (d) Schematic illustration of layer-by-layer silk fibroin-modified PCL nanofibers

clicked by MGF. (e) Representative SEM images of PCL, PCL/SF, and PCL/SF-MGF electrospun scaffolds showing fibers morphology. (f) Click chemistry and non-specific protein adsorption (without Cu^{2+} catalysis) of GFP-labeled MGF on layer-by-layer silk fibroin-modified PCL nanofibers scaffolds. Scale bar, 50 μm. Quantitative fluorescence density of MGF surface modified scaffolds after washed by PBS. *$p < 0.05$. Data are presented as the mean ± SD ($n = 4$).

3.6. In vitro modulation of macrophage polarization by MGF-functionalized electrospun fibers

We stained the macrophage cytoskeleton with FITC-phalloidin to observe the difference in cell morphology on different fibers (Fig. 6a). Macrophages generally adhere to the surface of electrospun fibers and grow along the direction of fibers arrangement, with a long spindle shape. Interestingly, the number of branches of macrophages was significantly lower in the MGF modified group compared with the PCL and PCL/SF groups (Fig. 6b). Macrophages with fewer pseudopodia means that they have less phagocytic behavior similar to the inactive M1 type state. Given the principal observation that MGF caused the macrophages polarization, we used real-time RT-PCR and immunofluorescence staining to investigate the effects of different surface-modified electrospun fibers. The gene and protein expression of M1 markers CD86, IL-23α, and iNOS, and the M2 markers CD163, CD206, and Arg-1 were detected after 72 h (Fig. 6c and d). According to the statistical analysis of the fluorescence images, the number of $CD86^+$ M1 macrophages was highest in the PCL group compared with the PCL/SF-MGF group but there was no significant difference in the number of iNOS positive macrophages among the groups. (Fig. 6e). The number of M2 macrophages were detected at high levels on the scaffolds with modified MGF (Fig. 6f). The expression levels of M2 surface markers were also high in the PCL/SF group, indicating that the surface modification of SF also could promoted the M2 phenotype transition of macrophages. Our findings suggested that MGF modified electrospun fibers can effectively regulate the transition of macrophages to M2 phenotype.

3.7. Foreign body response to MGF-functionalized electrospun fibers

Foreign body reaction is an inevitable immune response when biomaterials implanted into the body, which determines the long-term survival and functions maintenance of materials. To identify the FBR to the MGF-modified PCL fibers, nanofibrous scaffolds were implanted subcutaneously in Sprague-Dawley rats for 4 weeks. Masson's trichrome staining was performed to analysis the collagenous fibrotic capsule formation at different points in time. The collagenous fibrotic capsule caused by the FBR hinders the communication between materials and host, which is the most important factor affecting the functions of implanted biomaterials. The results showed that the thickest collagen fibrotic capsules (approximately 156 μm) appeared in the PCL group after 14 days and 28 days implantation compared with the PCL/SF and PCL/SF-MGF groups (Fig. 7a, left column and 7c). The surface LBL modification of silk can significantly reduce the thickness of the fibrotic capsule compared with the PCL group at 14 and 28 days after implantation (Fig. 7a, middle column). Importantly, PCL/SF-MGF scaffold exhibit significantly decreased fibrotic capsule thickness after 28 days implantation compared with the PCL and PCL/SF groups. We also found that the distribution of α-SMA positive cells representing myofibroblasts also showed similar results (Fig. 7b). To further determine whether the MGF-modified scaffold is capable to mitigate the FBR by regulating the macrophage phenotype, we used serial sections for immunofluorescence detection of M-pan (CD68), M1 (CCR7) and M2 (Arg-1) surface markers of macrophages after 28 days implantation. The serial sections offer an opportunity to detect the macrophages at a same area. As Fig. 7d and e shown, compare with PCL and PCL/SF scaffolds, the number of $CD68^+$/$Arg\text{-}1^+$ macrophages increased significantly in PCL/SF-MGF scaffold, but $CD68^+$/$Arg\text{-}1^+$ macrophages have seldom change. The results show that MGF-functionalized electrospun fibers can effectively increase the ratio of M2/M1 *in vivo*, which may be the main reason for its reduction of the FBR.

(a) Representative images of the Masson's Trichrome staining of histological sections of different nanofibrous scaffolds after 14 and 28 days of subcutaneous implantation and (b) α-SMA immunofluorescent staining of histological sections of different nanofibrous scaffolds after 28 days of subcutaneous implantation. (c) Analysis of the thickness of the fibrotic capsule surrounding the different scaffolds. *$p < 0.05$. Data are presented as the mean ± SD ($n = 8$). (d) Representative images of immunofluorescent staining for CD68, CCR7 and Arg-1 on continuous sections of different nanofibrous scaffolds after 14 days. (e) Analysis the $Arg\text{-}1^+/CCR7^+$ ratio of histological sections after 14 days of subcutaneous implantation. The "S" mark means the Scaffolds, and the dashed line means the location of the interface between the scaffold and the tissue. to represent the position of the scaffolds. *$p < 0.05$. Data are presented as the mean ± SD ($n = 8$).

3.8. MGF-functionalized electrospun scaffold prevents tendon adhesion

To further test the application effect of MGF-functionalized electrospun scaffold, we established a rat model of tendon adhesion as Fig. 8a and Supplementary Fig. 9 shown. The tendon adhesion was detected and assessed by analysis the by direct observation and Masson's trichrome staining. After 7 days of implantation, no obvious signs of inflammation or ulcer around the incision were discovered. However, the tendon adhesions around implanted zones can be detected by direct observation in PCL and PCL/SF groups (Fig. 8b). In addition, the tendon adhesions severely aggravate in PCL groups at day 14 and day 28 after implantation. Interestingly, the anti-adhesion effect was pronounced in the PCL/SF-MGF group. Little adhesion can be observed between the peritendinous tissue and the tendon at day 28 after implantation, and the scaffold can flexible lateral movement. The results imply that PCL/SF-MGF scaffold may possess strong antiadhesive capability. Additionally, histological sections of the tendons wrapped with scaffolds showed that a mass of fibrotic tissues (red arrow) appeared between the tendon and the PCL scaffold. In the PCL/SF group, loose bundles of fibrotic tissues could be found around the repaired tendon. We found that 28 days after implantation, almost no adhesion can be detected in the MGF-modified group, a sheath space formed between tendon and scaffold. These results indicate that the PCL/SF-MGF scaffold hinders the formation of fibrotic tissue and shows great potential as an anti-adhesion biomaterial (Fig. 8c and Supplementary Fig. 10).

(a) Schematic illustration of the *in vivo* anti-adhesion experiments surgical process in a rat model of tendon adhesion. (b) Gross evaluation of the rat Achilles's tendon wrapped with PCL, PCL/SF, and PCL/SF-MGF scaffolds after 14 and 28 days of scaffolds implantation. (c) Representative images of the Masson's Trichrome staining of histological sections of different nanofibrous scaffolds after 7, 14 and 28 days of implantation. Green arrows indicate the sheath space between the tendon and scaffolds, while red arrows indicate fibrosis tissue adhesions between the tendon and scaffolds.

4. Discussion

It is wildly understanding that growth factors have potentials to regulate macrophage polarization, such as IGF-1 can driving macrophages to the anti-inflammatory phenotype [41]. As an alternative splicing product of IGF-1, the short peptide MGF involves a series of tissue repair process, especially in connect tissues such as tendon and ligament [42]. Except to promote cell proliferation and migration, MGF also can regulate cell phenotype transition such as stem cell differentiation [43]. In regulating immune response, *in vivo* studies prove that MGF possesses strong anti-inflammation capability in repairing rat tendon injury and preventing rabbit osteoarthritis [36]. *In vitro* study further reported that MGF can reduce the pro-inflammatory cytokine

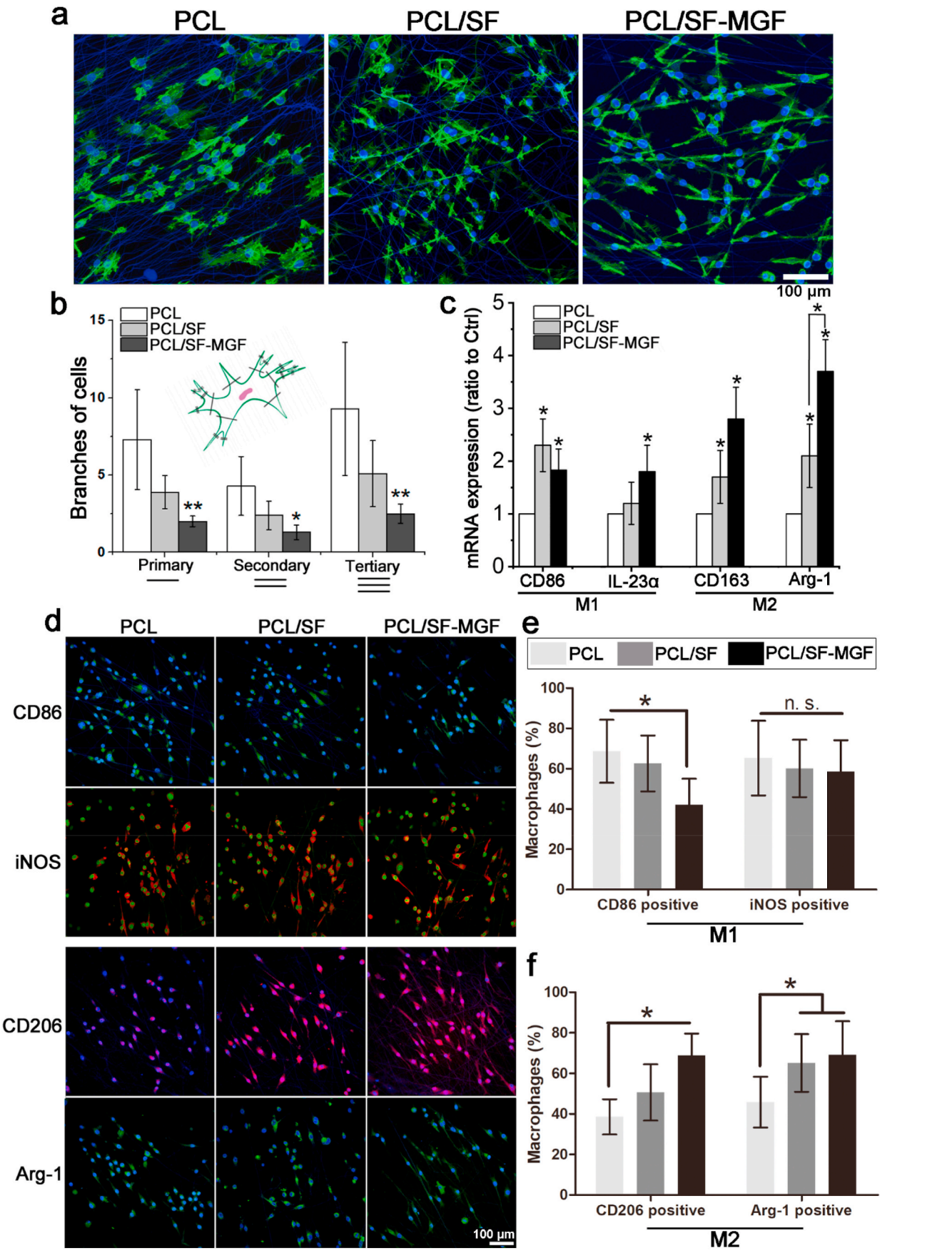

(caption on next page)

Fig. 6. *In vitro* modulation of macrophage polarization by MGF-functionalized electrospun fibers. (a) Cell morphology was stained by Alexa Fluor 488-phalloidin after cultured on PCL, PCL/SF, and PCL/SF-MGF nanofibrous scaffolds for 24 h. (b) Cell branches analysis of macrophages cultured on different scaffolds. *$p < 0.05$, **$p < 0.01$. Data are presented as the mean ± SD (n = 3). (c) Gene expression of CD86, IL-23α, CD163 and Arg-1 in macrophages after 12 h of culture with different scaffolds. Results were normalized to an endogenous control gene (GAPDH) and expression relative to non-treatment group. *$p < 0.05$. Data are presented as the mean ± SD (n = 3). (d) Immunofluorescent images of macrophages stained with pro-inflammation phenotype markers CD86 and iNOS, and anti-inflammation phenotype markers CD206 and Arg-1 cultured on different scaffolds for 24 h. Scale bar, 50 μm. (e) and (f) Image analysis the percentages of $CD86^+$ and $iNOS^+$ pro-inflammatory macrophages and $CD206^+$ and $Arg\text{-}1^+$ anti-inflammatory macrophages cultured on different scaffolds. *$p < 0.05$. Data are presented as the mean ± SD (n = 3).

expression in human fibroblast-like synoviocytes of knee osteoarthritis such as IL-1β and TNF-α [35]. For the first time, this work demonstrates that MGF can regulate the macrophage polarization by driving pan-macrophage transition into an anti-inflammatory phenotype. It is already well understanding that STAT6 is a key factor to drive macrophage anti-inflammatory polarization [44]. Our results demonstrate that MGF is capable to induce STAT6 expression and promote STAT6 relocation from cytoplasm to nucleus to direct an anti-inflammatory phenotype (M2) transition but not pro-inflammatory phenotype (M1) in macrophages. At the same time, STAT6 knockdown will block the effect of MGF in regulating macrophage polarization, such as promote the IL-10 secretion (Supplementary Fig. 6). In addition, MGF cannot induce STAT6 expression in HAT-inhibited macrophages, and HDAC inhabitation can further promote STAT6 expression in macrophages (Supplementary Fig. 7). Indeed, STAT6 act as a core mediator and activator during macrophage polarization mediates the transcriptional activation of anti-inflammatory macrophage-specific genes such as arginase 1 (Arg 1) and mannose receptor 1 (Mrc1), which also involves pathways especially the IL-4/STAT6 pathway to promote the macrophages polarized to M2 phenotype [45,46]. This imply that MGF may share the similar cell signaling cascade with IL-4 to regulate macrophages polarization. However, macrophages response IL-4 stimuli via the specific receptor-IL-4Rα, but the response of MGF was based on the endocytosis, which suggested that there should have a uniform upstream to regulate the STAT6 expression [47]. We supposed that it could correlate with epigenetic modification.

The cell phenotypic transition coupled with epigenetic state changes are well understood such as somatic cell reprogramming and stem cell differentiation [48,49]. Pre-existing chromatin marks deposited during macrophage polarization can be used to interpret, calibrate, and transmit exogenous signals to determine the magnitude and specificity of gene expression, and ultimately determine the macrophage phenotypes [50]. MGF increases the histone acetylation in macrophages, which induces a more “open” chromatin state and promotes the accessibility of transcription complexes to genomic DNA and further regulation of gene expression. This process decreases the “energy barrier” between pan-macrophage to the functional macrophage phenotypes. Concerning regulating histone acetylation to affect cell phenotype transition, both reduce HDAC and raise HAT are potential mechanisms. By reducing the histone deacetylation to regulate macrophage polarization into anti-inflammatory phenotype are wildly understand. For example, IL-4-activated STAT6 act as a transcriptional repressor in HDAC3-dependent macrophage polarization [51], and HDAC3 acts as a brake on IL-4-induced M2 polarization by deacetylating putative enhancers of IL-4-induced M2 genes [50,52]. Also, the inhibition of HDAC6 activity can limit the LPS-induced macrophage activation and secretion of proinflammatory cytokines [53]. The present study finds that MGF could decrease the HDAC activity, which is consistent with previous study. However, whether the mechanism of promote anti-inflammatory phenotype transition is similar between MGF and IL-4 still need to further study. In sum, MGF induces the histone acetylation and promotes the STAT6 expression, which increases the opportunity of pan-macrophages transition into anti-inflammatory phenotype.

In addition to the analysis of key signaling pathways, we analysis that the morphology of macrophages changed after MGF treatment. The macrophages showed an elongated morphology and the spread area decreased (Fig. 1d). Macrophages also showed morphological changes similar to 2D culture on the surface of the MGF functionalized electrospinning scaffold, and the protruding of pseudopodia also decreased significantly (Fig. 6a and b). It is worth noting that the morphologies and phenotypes of macrophages are closely related. For example, lipopolysaccharide (LPS) can activate the Toll-like receptor (TLR) signaling cascade to convert macrophages to the M1 phenotype, and can promote the spread of macrophages and pseudopodia by regulating actin polymerization [54]. However, limiting the spread of macrophages can promote the transformation of LPS activated M1 macrophages to M2 phenotype [55]. On the other hand, cell elongation is also important for macrophage M2 polarization. For example, based on a 20 μm wide micropatterned substrate promote cell elongation and prime these cells for differentiation into M2 phenotype compared with flat substrate [13]. Although the mechanism is not clear, MGF can prolong macrophage morphology and decline spreading area and pseudopodia in both 2D and 3D conditions, which is beneficial to the activation of M2 phenotype.

Advantages of MGF has been reported in tissue repair and anti-inflammation. Also, as a short peptide MGF performed a low cost in industry fabrication. However, there are still few studies on MGF as an immunomodulatory factor combined with biomaterials for clinical applications. Due to the high specific surface area and the fibrous structure similar to the extracellular matrix, the electrospun scaffold as a carrier for drug delivery offers an opportunity to utilize the MGF for the immunomodulatory function during implantation. However, electrospun micro/nanofibrous scaffold based on synthetic polymers often causes the FBR after implantation, and the formed collagen fibrotic capsules hinder its functions such as inducing tissue regeneration, drug delivery, and resisting tissue adhesion [21]. Currently, accumulating studies focus on the surface modification of biomaterials to reduce or prevent the FBR by regulating macrophage polarization. In our previous study, we developed SF surface-functionalized electrospun PCL fibers by single-component LbL assembly and decorated the SF with HD and IL-4 by diazonium coupling and click chemistry [28]. The scaffolds with immunomodulatory functions can regulate macrophage polarization at the tissue-implant interface and mitigate the FBR. Due to the biostability of silk LbL self-assembly and the specificity and efficiency of click chemistry, in this study, MGF was immobilized on the surface of PCL electrospun fiber using the same surface modification technologies. In a subcutaneous implantation model in rats, it can be found that the MGF-functionalized scaffold has a thinner fibrotic capsule at the tissue/material interface, fewer α-SMA positive myofibroblasts, and more M2 phenotype macrophages compared to the non-modified groups. These results indicate that MGF can effectively mitigate the FBR of materials by regulating the polarization of macrophages.

The clinical effect of the MGF modified scaffold is focused on preventing the tendon post-surgical adhesion in the present study. For most of the clinical attempts to prevent tissue adhesion, physical barriers were introduced after surgeries to create a protective shield between the wound and its surrounding tissues, thereby reducing the possibility of adhesion formation [56]. With this consideration, various physical barriers made from electrospun nanofibers scaffolds were developed [23,57,58]. Inhibiting excessive collagen deposition and fibroblasts/myofibroblasts proliferation are the primary approaches for preventing tissue adhesion. However, some drawbacks of these physical barriers were performed in anti-adhesion materials due to the biological functions were neglected when designing materials [59,60]. The biomaterials implanting will induce a series of immune events, especially

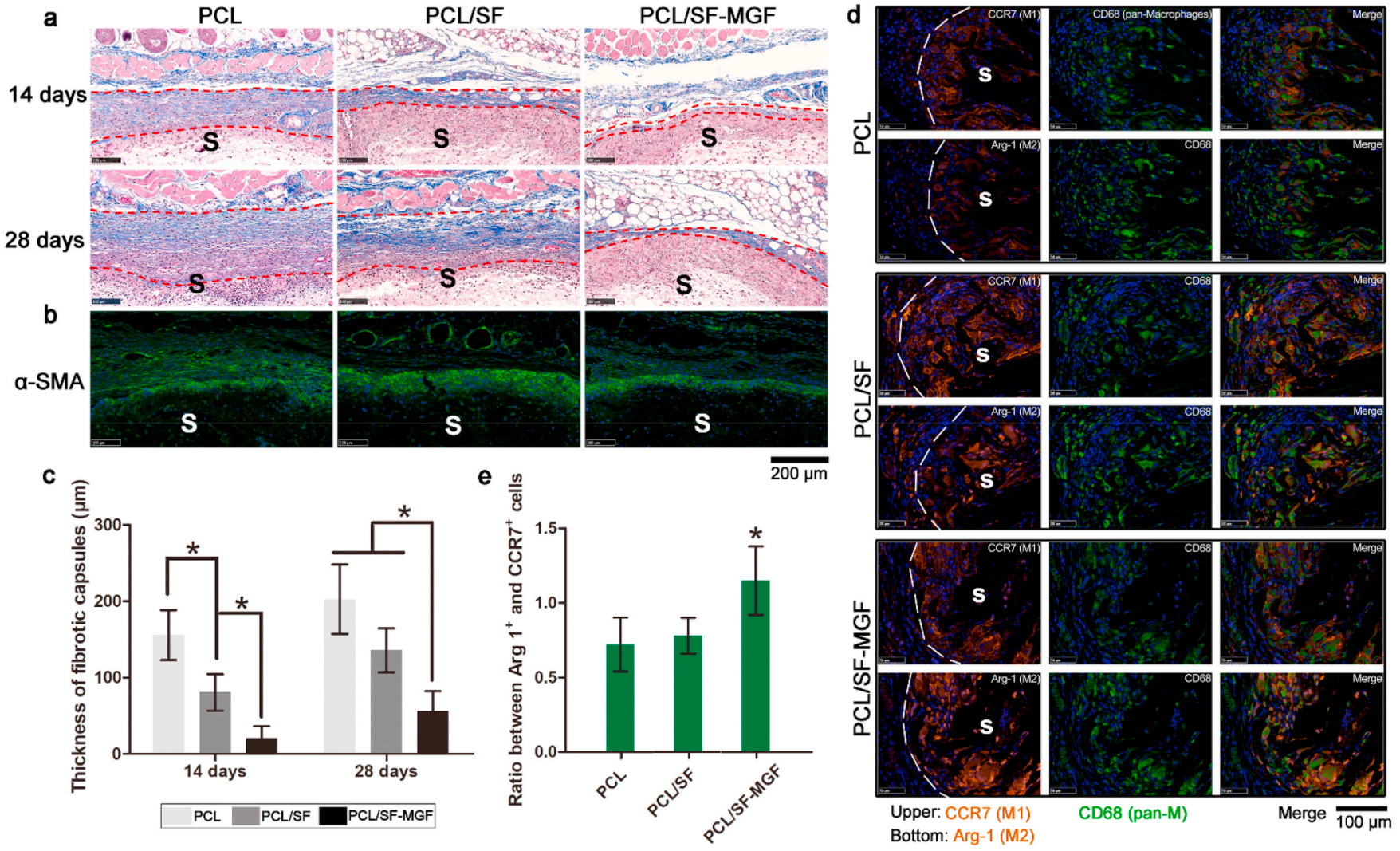

Fig. 7. Foreign -body response to MGF-functionalized electrospun fibers.

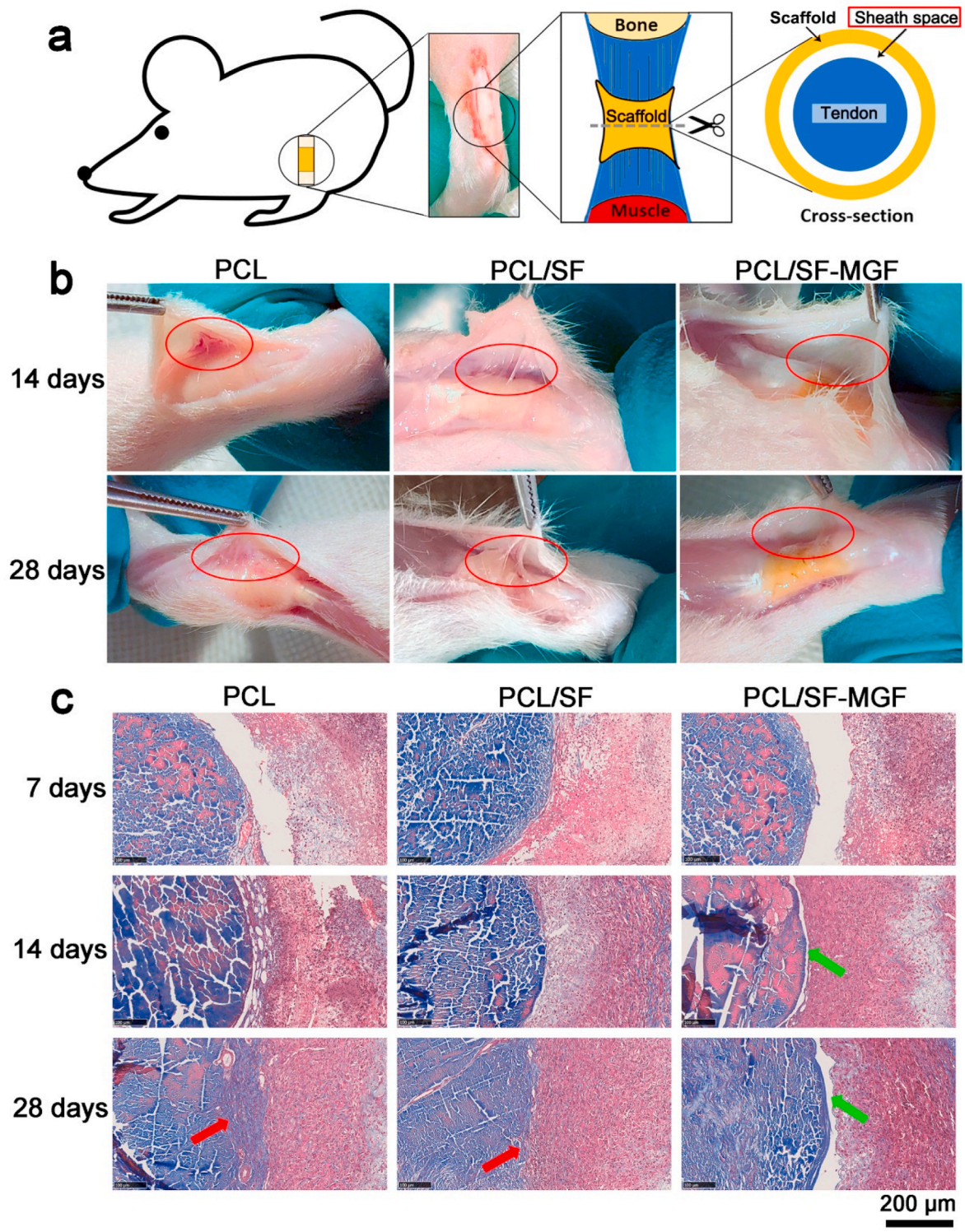

Fig. 8. MGF-functionalized electrospun scaffold prevents tendon adhesion.

the FBR, over-secreted cytokines and cell recruit broken the balance of tissue microenvironment and leading the tissue fibrosis, which will accelerate the formation of tissue adhesion [5,61]. Therefore, engineering functional biomaterials that combine biological, physical, and chemical effects will likely be more effective for post-surgical recovery. In this study, MGF functionalized electrospun nanofibrous scaffold can not only provide a physical barrier, more importantly, MGF is capable to greatly reduce the deposition of collagen fibrotic tissue by regulating the macrophage polarization to mitigate the FBR. Our results found that neither the subcutaneous peripheral tissue nor the tendon adhered to the MGF-functionalized scaffold, and a uniform sheath space was formed between the tendon and the scaffold.

5. Conclusions

In summary, the biological mechanism by which MGF directs the macrophages transformed into anti-inflammation M2 phenotype through promotes histone acetylation and enhances STAT6 expression

was discovered. Then, MGF surface functionalized electrospun PCL scaffold was fabricated using a SF single-component layer-by-layer assembly and click chemistry, resulting in the covalent binding of MGF with the capacity to modulate macrophage polarization *in vitro* and effectively downregulate the implantation induced the FBR *in vivo*. Finally, the MGF-modified scaffold as an anti-adhesion physical barrier with immunomodulatory ability has excellent performance in rat Achilles tendon injury adhesion model. This work is focused on studying the immunomodulatory function of MGF on macrophage polarization and its ability as a new immunomodulatory peptide can effectively mitigate the foreign body reactions of biomaterial and resist tissue adhesion.

CRediT authorship contribution statement

Yang Song: Conceptualization, Methodology, Software, Formal analysis, Investigation, Data curation, Writing – original draft. **Linhao Li:** Conceptualization, Methodology, Software, Writing – original draft, Supervision, Project administration, Funding acquisition. **Weikang Zhao:** Investigation, Data curation. **Yuna Qian:** Validation, Investigation, Data curation. **Lili Dong:** Investigation, Data curation. **Yunnan Fang:** Investigation, Data curation. **Li Yang:** Writing – review & editing, Supervision, Funding acquisition. **Yubo Fan:** Writing – review & editing, Supervision, Funding acquisition.

Declaration of competing interest

The authors declare no competing interests.

Acknowledgments

We acknowledge the funding support from the National Natural Science Foundation of China (31971258, 11532004), the 111 Project (B06023, B13003), and Chongqing Postdoctoral Science Foundation (csts2019jcyj-bsh0068).

Appendix A. Supplementary data

Supplementary data to this article can be found online at https://doi.org/10.1016/j.bioactmat.2021.02.020.

References

[1] B.D. Ratner, Biomaterials: been there, done that, and evolving into the future, Annu. Rev. Biomed. Eng. 21 (2019) 171–191, https://doi.org/10.1146/annurev-bioeng-062117-120940.
[2] A. Vishwakarma, N.S. Bhise, M.B. Evangelista, J. Rouwkema, M.R. Dokmeci, A. M. Ghaemmaghami, N.E. Vrana, A. Khademhosseini, Engineering immunomodulatory biomaterials to tune the inflammatory response, Trends Biotechnol. 34 (2016) 470–482, https://doi.org/10.1016/j.tibtech.2016.03.009.
[3] J.M. Anderson, A. Rodriguez, D.T. Chang, Foreign body reaction to biomaterials, Semin. Immunol. 20 (2008) 86–100, https://doi.org/10.1016/j.smim.2007.11.004.
[4] B.D. Ratner, Chapter 3 - the biocompatibility of implant materials, in: S.F. Badylak (Ed.), Host Response to Biomater, Academic Press, Oxford, 2015, pp. 37–51, https://doi.org/10.1016/B978-0-12-800196-7.00003-7.
[5] S. Al-Maawi, A. Orlowska, R. Sader, C. James Kirkpatrick, S. Ghanaati, In vivo cellular reactions to different biomaterials—physiological and pathological aspects and their consequences, Semin. Immunol. 29 (2017) 49–61, https://doi.org/10.1016/j.smim.2017.06.001.
[6] T.A. Wynn, K.M. Vannella, Macrophages in tissue repair, regeneration, and fibrosis, Immunity 44 (2016) 450–462, https://doi.org/10.1016/j.immuni.2016.02.015.
[7] N. Jain, J. Moeller, V. Vogel, Mechanobiology of macrophages: how physical factors coregulate macrophage plasticity and phagocytosis, Annu. Rev. Biomed. Eng. 21 (2019) 267–297, https://doi.org/10.1146/annurev-bioeng-062117-121224.
[8] C.K. Glass, G. Natoli, Molecular control of activation and priming in macrophages, Nat. Immunol. 17 (2016) 26–33, https://doi.org/10.1038/ni.3306.
[9] P.J. Murray, Macrophage polarization, Annu. Rev. Physiol. 79 (2017) 541–566, https://doi.org/10.1146/annurev-physiol-022516-034339.
[10] D. Hachim, S.T. LoPresti, C.C. Yates, B.N. Brown, Shifts in macrophage phenotype at the biomaterial interface via IL-4 eluting coatings are associated with improved implant integration, Biomaterials 112 (2017) 95–107, https://doi.org/10.1016/j.biomaterials.2016.10.019.
[11] T.M. Raimondo, D.J. Mooney, Functional muscle recovery with nanoparticle-directed M2 macrophage polarization in mice, Proc. Natl. Acad. Sci. U. S. A 115 (2018) 10648–10653, https://doi.org/10.1073/pnas.1806908115.
[12] L. Zhang, Z. Cao, T. Bai, L. Carr, J.-R. Ella-Menye, C. Irvin, B.D. Ratner, S. Jiang, Zwitterionic hydrogels implanted in mice resist the foreign-body reaction, Nat. Biotechnol. 31 (2013) 553–556, https://doi.org/10.1038/nbt.2580.
[13] F.Y. McWhorter, T. Wang, P. Nguyen, T. Chung, W.F. Liu, Modulation of macrophage phenotype by cell shape, Proc. Natl. Acad. Sci. U. S. A 110 (2013) 17253–17258, https://doi.org/10.1073/pnas.1308887110.
[14] M.J. Vassey, G.P. Figueredo, D.J. Scurr, A.S. Vasilevich, S. Vermeulen, A. Carlier, J. Luckett, N.R.M. Beijer, P. Williams, D.A. Winkler, J. de Boer, A. M. Ghaemmaghami, M.R. Alexander, Immune modulation by design: using topography to control human monocyte attachment and macrophage differentiation, Adv. Sci. (Weinheim, Baden-Wurttemberg, Ger. 7 (2020) 1903392, https://doi.org/10.1002/advs.201903392.
[15] E.M. Sussman, M.C. Halpin, J. Muster, R.T. Moon, B.D. Ratner, Porous implants modulate healing and induce shifts in local macrophage polarization in the foreign body reaction, Ann. Biomed. Eng. 42 (2014) 1508–1516, https://doi.org/10.1007/s10439-013-0933-0.
[16] O. Veiseh, J.C. Doloff, M. Ma, A.J. Vegas, H.H. Tam, A.R. Bader, J. Li, E. Langan, J. Wyckoff, W.S. Loo, S. Jhunjhunwala, A. Chiu, S. Siebert, K. Tang, J. Hollister-Lock, S. Aresta-Dasilva, M. Bochenek, J. Mendoza-Elias, Y. Wang, M. Qi, D. M. Lavin, M. Chen, N. Dholakia, R. Thakrar, I. Lacík, G.C. Weir, J. Oberholzer, D. L. Greiner, R. Langer, D.G. Anderson, Size- and shape-dependent foreign body immune response to materials implanted in rodents and non-human primates, Nat. Mater. 14 (2015) 643–651, https://doi.org/10.1038/nmat4290.
[17] Y. Dong, Y. Zheng, K. Zhang, Y. Yao, L. Wang, X. Li, J. Yu, B. Ding, Electrospun nanofibrous materials for wound healing, Adv. Fiber Mater. 2 (2020) 212–227, https://doi.org/10.1007/s42765-020-00034-y.
[18] W. Huang, Y. Xiao, X. Shi, Construction of electrospun organic/inorganic hybrid nanofibers for drug delivery and tissue engineering applications, Adv. Fiber Mater 1 (2019) 32–45, https://doi.org/10.1007/s42765-019-00007-w.
[19] T.J. Sill, H.A. von Recum, Electrospinning: applications in drug delivery and tissue engineering, Biomaterials 29 (2008) 1989–2006, https://doi.org/10.1016/j.biomaterials.2008.01.011.
[20] K.M. Woo, V.J. Chen, P.X. Ma, Nano-fibrous scaffolding architecture selectively enhances protein adsorption contributing to cell attachment, J. Biomed. Mater. Res. A. 67 (2003) 531–537, https://doi.org/10.1002/jbm.a.10098.
[21] S. Lucke, U. Walschus, A. Hoene, M. Schnabelrauch, J.B. Nebe, B. Finke, M. Schlosser, The in vivo inflammatory and foreign body giant cell response against different poly(l-lactide-co-d/l-lactide) implants is primarily determined by material morphology rather than surface chemistry, J. Biomed. Mater. Res. A. 106 (2018) 2726–2734, https://doi.org/10.1002/jbm.a.36500.
[22] D. Grafahrend, K.-H. Heffels, M.V. Beer, P. Gasteier, M. Möller, G. Boehm, P. D. Dalton, J. Groll, Degradable polyester scaffolds with controlled surface chemistry combining minimal protein adsorption with specific bioactivation, Nat. Mater. 10 (2011) 67–73, https://doi.org/10.1038/nmat2904.
[23] L. Cheng, Y. Wang, G. Sun, S. Wen, L. Deng, H. Zhang, W. Cui, Hydration-enhanced lubricating electrospun nanofibrous membranes prevent tissue adhesion, Res. 2020 (2020) 4907185, https://doi.org/10.34133/2020/4907185.
[24] W. Yang, H.S. Sundaram, J.-R. Ella, N. He, S. Jiang, Low-fouling electrospun PLLA films modified with zwitterionic poly(sulfobetaine methacrylate)-catechol conjugates, Acta Biomater. 40 (2016) 92–99, https://doi.org/10.1016/j.actbio.2016.05.035.
[25] Z. Wang, Y. Cui, J. Wang, X. Yang, Y. Wu, K. Wang, X. Gao, D. Li, Y. Li, X.-L. Zheng, Y. Zhu, D. Kong, Q. Zhao, The effect of thick fibers and large pores of electrospun poly(ε-caprolactone) vascular grafts on macrophage polarization and arterial regeneration, Biomaterials 35 (2014) 5700–5710, https://doi.org/10.1016/j.biomaterials.2014.03.078.
[26] A.D. Schoenenberger, H. Tempfer, C. Lehner, J. Egloff, M. Mauracher, A. Bird, J. Widmer, K. Maniura-Weber, S.F. Fucentese, A. Traweger, U. Silvan, J. G. Snedeker, Macromechanics and polycaprolactone fiber organization drive macrophage polarization and regulate inflammatory activation of tendon in vitro and in vivo, Biomaterials 249 (2020) 120034, https://doi.org/10.1016/j.biomaterials.2020.120034.
[27] L. Li, Y. Qian, C. Jiang, Y. Lv, W. Liu, L. Zhong, K. Cai, S. Li, L. Yang, The use of hyaluronan to regulate protein adsorption and cell infiltration in nanofibrous scaffolds, Biomaterials 33 (2012) 3428–3445, https://doi.org/10.1016/j.biomaterials.2012.01.038.
[28] Y. Qian, L. Li, Y. Song, L. Dong, P. Chen, X. Li, K. Cai, O. Germershaus, L. Yang, Y. Fan, Surface modification of nanofibrous matrices via layer-by-layer functionalized silk assembly for mitigating the foreign body reaction, Biomaterials 164 (2018) 22–37, https://doi.org/10.1016/j.biomaterials.2018.02.038.
[29] K. Iida, E. Itoh, D.-S. Kim, J.P. del Rincon, K.T. Coschigano, J.J. Kopchick, M. O. Thorner, Muscle mechano growth factor is preferentially induced by growth hormone in growth hormone-deficient lit/lit mice, J. Physiol. 560 (2004) 341–349, https://doi.org/10.1113/jphysiol.2004.069500.
[30] R.W.J. Matheny, B.C. Nindl, M.L. Adamo, Minireview: mechano-growth factor: a putative product of IGF-I gene expression involved in tissue repair and regeneration, Endocrinology 151 (2010) 865–875, https://doi.org/10.1210/en.2009-1217.
[31] M. Deng, B. Zhang, K. Wang, F. Liu, H. Xiao, J. Zhao, P. Liu, Y. Li, F. Lin, Y. Wang, Mechano growth factor E peptide promotes osteoblasts proliferation and bone-

defect healing in rabbits, Int. Orthop. 35 (2011) 1099–1106, https://doi.org/10.1007/s00264-010-1141-2.
[32] Z. Luo, L. Jiang, Y. Xu, H. Li, W. Xu, S. Wu, Y. Wang, Z. Tang, Y. Lv, L. Yang, Mechano growth factor (MGF) and transforming growth factor (TGF)-β3 functionalized silk scaffolds enhance articular hyaline cartilage regeneration in rabbit model, Biomaterials 52 (2015) 463–475, https://doi.org/10.1016/j.biomaterials.2015.01.001.
[33] L.-L. Qin, X.-K. Li, J. Xu, D.-L. Mo, X. Tong, Z.-C. Pan, J.-Q. Li, Y.-S. Chen, Z. Zhang, C. Wang, Q.-M. Long, Mechano growth factor (MGF) promotes proliferation and inhibits differentiation of porcine satellite cells (PSCs) by down-regulation of key myogenic transcriptional factors, Mol. Cell. Biochem. 370 (2012) 221–230, https://doi.org/10.1007/s11010-012-1413-9.
[34] B. Zhang, Q. Luo, Z. Chen, Y. Shi, Y. Ju, L. Yang, G. Song, Increased nuclear stiffness via FAK-ERK1/2 signaling is necessary for synthetic mechano-growth factor E peptide-induced tenocyte migration, Sci. Rep. 6 (2016) 18809, https://doi.org/10.1038/srep18809.
[35] H. Li, M. Lei, C. Yu, Y. Lv, Y. Song, L. Yang, Mechano growth factor-E regulates apoptosis and inflammatory responses in fibroblast-like synoviocytes of knee osteoarthritis, Int. Orthop. 39 (2015) 2503–2509, https://doi.org/10.1007/s00264-015-2974-5.
[36] Y. Song, K. Xu, C. Yu, L. Dong, P. Chen, Y. Lv, M.Y.M. Chiang, L. Li, W. Liu, L. Yang, The use of mechano growth factor to prevent cartilage degeneration in knee osteoarthritis, J. Tissue Eng. Regen. Med. 12 (2018), https://doi.org/10.1002/term.2493.
[37] L. Li, S. Puhl, L. Meinel, O. Germershaus, Silk fibroin layer-by-layer microcapsules for localized gene delivery, Biomaterials 35 (2014) 7929–7939, https://doi.org/10.1016/j.biomaterials.2014.05.062.
[38] J.E. Moses, A.D. Moorhouse, The growing applications of click chemistry, Chem. Soc. Rev. 36 (2007) 1249–1262, https://doi.org/10.1039/b613014n.
[39] H. Zhao, E. Heusler, G. Jones, L. Li, V. Werner, O. Germershaus, J. Ritzer, T. Luehmann, L. Meinel, Decoration of silk fibroin by click chemistry for biomedical application, J. Struct. Biol. 186 (2014), https://doi.org/10.1016/j.jsb.2014.02.009.
[40] Y. Jiang, J. Chen, C. Deng, E.J. Suuronen, Z. Zhong, Click hydrogels, microgels and nanogels: emerging platforms for drug delivery and tissue engineering, Biomaterials 35 (2014) 4969–4985, https://doi.org/10.1016/j.biomaterials.2014.03.001.
[41] O. Spadaro, C.D. Camell, L. Bosurgi, K.Y. Nguyen, Y.-H. Youm, C.V. Rothlin, V. D. Dixit, IGF1 shapes macrophage activation in response to immunometabolic challenge, Cell Rep. 19 (2017) 225–234, https://doi.org/10.1016/j.celrep.2017.03.046.
[42] B. Zhang, Q. Luo, X. Mao, B. Xu, L. Yang, Y. Ju, G. Song, A synthetic mechano-growth factor E peptide promotes rat tenocyte migration by lessening cell stiffness and increasing F-actin formation via the FAK-ERK1/2 signaling pathway, Exp. Cell Res. 322 (2014) 208–216, https://doi.org/10.1016/j.yexcr.2014.01.005.
[43] H. Cui, Q. Yi, J. Feng, L. Yang, L. Tang, Mechano growth factor E peptide regulates migration and differentiation of bone marrow mesenchymal stem cells, J. Mol. Endocrinol. 52 (2014) 111–120, https://doi.org/10.1530/JME-13-0157.
[44] T. Yu, S. Gan, Q. Zhu, D. Dai, N. Li, H. Wang, X. Chen, D. Hou, Y. Wang, Q. Pan, J. Xu, X. Zhang, J. Liu, S. Pei, C. Peng, P. Wu, S. Romano, C. Mao, M. Huang, X. Zhu, K. Shen, J. Qin, Y. Xiao, Modulation of M2 macrophage polarization by the crosstalk between Stat6 and Trim 24, Nat. Commun. 10 (2019) 4353, https://doi.org/10.1038/s41467-019-12384-2.
[45] S. Nepal, C. Tiruppathi, Y. Tsukasaki, J. Farahany, M. Mittal, J. Rehman, D. J. Prockop, A.B. Malik, STAT6 induces expression of Gas6 in macrophages to clear apoptotic neutrophils and resolve inflammation, Proc. Natl. Acad. Sci. U. S. A 116 (2019) 16513–16518, https://doi.org/10.1073/pnas.1821601116.
[46] M. Sanson, E. Distel, E.A. Fisher, HDL induces the expression of the M2 macrophage markers arginase 1 and Fizz-1 in a STAT6-dependent process, PloS One 8 (2013), e74676, https://doi.org/10.1371/journal.pone.0074676.
[47] S.-Y. Weng, X. Wang, S. Vijayan, Y. Tang, Y.O. Kim, K. Padberg, T. Regen, O. Molokanova, T. Chen, T. Bopp, H. Schild, F. Brombacher, J.R. Crosby, M. L. McCaleb, A. Waisman, E. Bockamp, D. Schuppan, IL-4 receptor alpha signaling through macrophages differentially regulates liver fibrosis progression and reversal, EBioMedicine 29 (2018) 92–103, https://doi.org/10.1016/j.ebiom.2018.01.028.
[48] D. Iliopoulos, H.A. Hirsch, K. Struhl, An epigenetic switch involving NF-kappaB, Lin 28, Let-7 MicroRNA, and IL6 links inflammation to cell transformation, Cell 139 (2009) 693–706, https://doi.org/10.1016/j.cell.2009.10.014.
[49] P. Wang, C. Song, H. Zhang, Z. Wu, X.-J. Tian, J. Xing, Epigenetic state network approach for describing cell phenotypic transitions, Interface Focus 4 (2014) 20130068, https://doi.org/10.1098/rsfs.2013.0068.
[50] L.B. Ivashkiv, Epigenetic regulation of macrophage polarization and function, Trends Immunol. 34 (2013) 216–223, https://doi.org/10.1016/j.it.2012.11.001.
[51] Z. Czimmerer, B. Daniel, A. Horvath, D. Rückerl, G. Nagy, M. Kiss, M. Peloquin, M. M. Budai, I. Cuaranta-Monroy, Z. Simandi, L. Steiner, B.J. Nagy, S. Poliska, C. Banko, Z. Bacso, I.G. Schulman, S. Sauer, J.-F. Deleuze, J.E. Allen, S. Benko, L. Nagy, The transcription factor STAT6 mediates direct repression of inflammatory enhancers and limits activation of alternatively polarized macrophages, Immunity 48 (2018) 75–90, https://doi.org/10.1016/j.immuni.2017.12.010, e6.
[52] S.E. Mullican, C.A. Gaddis, T. Alenghat, M.G. Nair, P.R. Giacomin, L.J. Everett, D. Feng, D.J. Steger, J. Schug, D. Artis, M.A. Lazar, Histone deacetylase 3 is an epigenomic brake in macrophage alternative activation, Genes Dev. 25 (2011) 2480–2488, https://doi.org/10.1101/gad.175950.111.
[53] S. Chen, J. Yang, Y. Wei, X. Wei, Epigenetic regulation of macrophages: from homeostasis maintenance to host defense, Cell. Mol. Immunol. 17 (2020) 36–49, https://doi.org/10.1038/s41423-019-0315-0.
[54] H. Shinji, K.S. Akagawa, T. Yoshida, Cytochalasin D inhibits lipopolysaccharide-induced tumor necrosis factor production in macrophages, J. Leukoc. Biol. 54 (1993) 336–342, https://doi.org/10.1002/jlb.54.4.336.
[55] N. Jain, V. Vogel, Spatial confinement downsizes the inflammatory response of macrophages, Nat. Mater. 17 (2018) 1134–1144, https://doi.org/10.1038/s41563-018-0190-6.
[56] W. Wu, R. Cheng, J. das Neves, J. Tang, J. Xiao, Q. Ni, X. Liu, G. Pan, D. Li, W. Cui, B. Sarmento, Advances in biomaterials for preventing tissue adhesion, J. Contr. Release 261 (2017) 318–336, https://doi.org/10.1016/j.jconrel.2017.06.020.
[57] Y. Wang, L. Cheng, S. Wen, S. Zhou, Z. Wang, L. Deng, H.-Q. Mao, W. Cui, H. Zhang, Ice-inspired superlubricated electrospun nanofibrous membrane for preventing tissue adhesion, Nano Lett. 20 (2020) 6420–6428, https://doi.org/10.1021/acs.nanolett.0c01990.
[58] K.T. Shalumon, C. Sheu, C.-H. Chen, S.-H. Chen, G. Jose, C.-Y. Kuo, J.-P. Chen, Multi-functional electrospun antibacterial core-shell nanofibrous membranes for prolonged prevention of post-surgical tendon adhesion and inflammation, Acta Biomater. 72 (2018) 121–136, https://doi.org/10.1016/j.actbio.2018.03.044.
[59] S. Jiang, X. Zhao, S. Chen, G. Pan, J. Song, N. He, F. Li, W. Cui, C. Fan, Down-regulating ERK1/2 and SMAD2/3 phosphorylation by physical barrier of celecoxib-loaded electrospun fibrous membranes prevents tendon adhesions, Biomaterials 35 (2014) 9920–9929, https://doi.org/10.1016/j.biomaterials.2014.08.028.
[60] H. Nakagawa, Y. Matsumoto, Y. Matsumoto, Y. Miwa, Y. Nagasaki, Design of high-performance anti-adhesion agent using injectable gel with an anti-oxidative stress function, Biomaterials 69 (2015) 165–173, https://doi.org/10.1016/j.biomaterials.2015.08.018.
[61] J.M. Anderson, A. Rodriguez, D.T. Chang, Foreign body reaction to biomaterials, Semin. Immunol. 20 (2008) 86–100, https://doi.org/10.1016/J.SMIM.2007.11.004.